ASYMMETRIC PLASMONIC NANO-BOWTIES FOR ELECTROMAGNETIC ENHANCEMENT

A DISSERTATION

SUBMITTED IN PARTIAL FULFILLMENT OF THE REQUIREMENTS
FOR THE AWARD OF DEGREE
OF

MASTER OF TECHNOLOGY
IN
MICROWAVE AND OPTICAL COMMUNICATION

Submitted by:

Vaibhav Sapra

2K17/MOC/09

Under the supervision of

DR. YASHNA SHARMA

DEPARTMENT OF ELECTRONICS AND COMMUNICATION ENGINEERING
DELHI TECHNOLOGICAL UNIVERSITY
(Formerly Delhi College of Engineering)
Bawana Road, Delhi-110042

JULY, 2019

DELHI TECHNOLOGICAL UNIVERSITY
(Formerly Delhi College of Engineering)
Bawana Road, Delhi-110042

CANDIDATE'S DECLARATION

I, Vaibhav Sapra, Roll No. 2K17/MOC/09, student of M.Tech (Microwave and Optical Communication), hereby declare that the project Dissertation titled "Asymmetric Plasmonic Nano-Bowties for Electromagnetic Enhancement" which is submitted by me to the department of Electronics and Communication Engineering, Delhi Technological University, Delhi in partial fulfilment of the requirement for the award of the degree of degree of Master of Technology, is original and not copied from any source without proper citation. This work has not previously formed the basis for the award of any Degree, Diploma Associateship, Fellowship or other similar title or recognition.

Place: Delhi **VAIBHAV SAPRA**

Date:

DEPARTMENT OF ELECTRONICS AND COMMUNICATION ENGINEERING
DELHI TECHNOLOGICAL UNIVERSITY
(Formerly Delhi College of Engineering)
Bawana Road, Delhi-110042

CERTIFICATE

I hereby certify that the project dissertation titled "Asymmetric Plasmonic Nano-Bowties for Electromagnetic Enhancement" which is submitted by Vaibhav Sapra, Roll No. 2K17/MOC/09, Department of Electronics and Communication Engineering, Delhi Technological University, Delhi in partial fulfilment of the requirement for the award of the degree of Master of Technology, is a record of the project work carried out by the student under my supervision. To the best of my knowledge this work has not been submitted in part or full for any Degree or Diploma to this University or elsewhere.

Place: Delhi
Date:

DR. YASHNA SHARMA
SUPERVISOR
(Assistant Professor, Department of Electronics and Communication Engineering, Delhi Technological University, Bawana Road, Delhi-110042)

ABSTRACT

Plasmonic nanostructures, which are properly engineered, lead to the phenomenon of localized surface plasmon resonance (LSPR), wherein, an enhance electric field near the surface of metal nanoparticles at the plasmon resonance wavelength can be observed. This phenomenon finds applications in many areas such as photo-voltaics, refractive index sensing and others. In this project, plasmonic nano-structures which offer high electromagnetic enhancement through the formation of EM hotspots, and due to the lightning rod effect are analyzed by employing Finite Difference Time Domain (FDTD) simulations. In the first part of the project, nano-spheres were simulated in an attempt to understand resonance and see the effect of introducing a second metal on the resonance spectrum. In the second part, the plasmonic properties of homo-structured bimetallic nano-bowties were exhaustively analyzed by varying different geometrical parameters. In the third part, the effect of breaking the symmetry of nano-bowties on the hybridized plasmonic modes created in these nanostructures will be simulated. The E-field enhancement will be calculated and the passive tunability of the plasmon resonance wavelength by varying the structural parameters will be numerically demonstrated.

ACKNOWLEDGEMENT

I have no words to thank Dr. Yashna Sharma, Department of Electronics & Communication Engineering, my supervisor, for her colossal and valuable support. The resources and the motivation provided by her were the reason for this endeavour to take shape. Her immense knowledge and infinite patience were my two supporting pillars.

I would also like to exhibit my appreciation to all friends and well wishers for their time and effort.

Date: VAIBHAV SAPRA

CONTENTS

LIST OF FIGURES

LIST OF ABBREVIATIONS

SPR	Surface Plasmon Resonance
LSPR	Localized Surface Plasmon Resonance
FDTD	Finite Difference Time Domain
SERS	Surface Enhanced Raman Spectroscopy
TM	Transverse Magnetic
TE	Transverse Electric
SP	Surface Plasmon
SAM	Self-Assembled Monolayer
MUA	Mercaptoundecanoic Acid
OT	Octanethiol
ADDL	Amyloid Derived Diffusible Ligand
AFM	Atomic Force Microscopy
OTA	Ochratoxin A
LED	Light Emitting Diodes
SPPL	Single Photon Luminescence
MPPL	Multi-Photon Luminescence
TPPL	Two-Photon Photoluminescence
WLSC	White Light Super Continuum
E	Electric Field
H	Magnetic Field

PML	Perfectly Matched Layer
EM	Electro-magnetic
VS	Versus

CHAPTER 1
INTRODUCTION

1.1 PLASMONICS

Nano-photonics is the discipline that deals with interaction of light and matter on the nanometre scale [1]. This interaction occurs when light of a specific wavelength is incident on structures whose dimensions are nanometer scale [1]. Nanomaterials exhibit very different optical properties as compared to their bulk counterparts which gives rise to numerous interesting nano-phenomenon. However, coinage metals such as silver and gold exhibit unique optical phenomenon due to their special optical properties. The interaction of light with these materials gave rise to the field of 'Plasmonics'. The enhancement of optical phenomenon offered by such metallic nanostructures has led to their employment in a variety of novel applications such as sensors, optical waveguides and solar cells.

The study of interaction of light with metallic nanoparticles or nanostructures is termed as *'Plasmonics'* [1]. It is well known that gold and silver are the most widely used metals for plasmonics. This is due to the fact that metals are lossy and differed metals have varying degree of wavelength dependent losses associated with them [2]. These losses restrict the usage of metals other than the coinage metals for applications in the field of plasmonics. In the visible regime, these losses are the least for gold and silver making them the materials of choice for plasmonic applications.

The unique optical properties of metal nano-structures stem from their ability to sustain electron oscillations on their surface, which are known as surface plasmons [3-4]. Scientists, have conducted experiments to understand the intriguing optical properties of metal nanoparticles [3-4]. As an example, Michal Faraday in the 1850s prepared gold nanoparticle suspensions that reacted to acids in a similar fashion as bulk gold and changed colour when aggregation inducing agents were added [3-4].

Electron excitations at the interface of a dielectric and a metal are called Surface Plasmon Resonance, abbreviated as SPR. When metallic nanoparticles are present instead of a nanostructured surface these oscillations become localized or confined to the surface of the nanoparticle and are known as Localized Surface Plasmon Resonance, abbreviated as LSPR [5-6].

With the advent of newer lithography tools like the Electron Beam lithography [7], Focussed Ion Beam Milling [8], nanosphere lithography [9] and the Extreme-UV lithography [10], the fabrication of these metallic nanostructures with sub-20 nm gaps has been made inexpensive and the fabrication time has been reduced. This has stirred the employment of these plasmonic substrates for numerous industry applications.

1.2 RESEARCH OBJECTIVES

The primary objectives of this project are as follows:

- To review the phenomenon of Surface Plasmon Resonances (SPR) and Localized Surface Plasmon Resonance (LSPR) from a physical and mathematical perspective in metal nanostructures and nanoparticles respectively.
- To carry out an exhaustive literature survey of the different applications employing Surface Plasmon Resonances or LSPR
- To study the applicability of bimetallic nano-particles (nano-bowties) as efficient SPR sensors, and suggest optimized design parameters for maximum enhancement
- To simulate the passive tunability in spectral response of bimetallic nano-particles by varying different geometrical parameters using FDTD simulations
- To study the effect and efficiency of introducing asymmetry to these bimetallic nano-bowtie substrates on plasmonic enhancement
- Make conclusive arguments on the applicability of proposed substrates in physical applications.

CHAPTER 2
LITERATURE REVIEW

2.1 SURFACE PLASMON RESONANCE AND LOCALIZED SURFACE PLASMON RESONANCE

Surface Plasmon Resonance is the light-induced, oscillation of conduction electrons at the interface of a metal and a dielectric. The quanta of these oscillations are called surface plasmons. The requirement for Surface Plasmon Resonance involves the presence of materials with positive and negative permittivity across the opposite sides of the interface [11].

In order to understand the phenomenon of Surface Plasmon Resonance, we consider an electromagnetic wave travelling across a metal/dielectric interface. Assuming external charges to be 0, the corresponding wave equation will be given by:

$$\nabla^2 \boldsymbol{E} - \frac{\epsilon}{c^2}\frac{\partial^2 \boldsymbol{E}}{\partial t^2} = 0 \tag{2.1}$$

where, **E** is the electric field component of the wave, c is the speed of light and ϵ is the dielectric profile [11]. It is assumed that the dielectric profile is constant over distances of about one optical wavelength. We assume the electric field to have the form,

$$\boldsymbol{E}(x, y, z, t) = \boldsymbol{E}(x, y, z)e^{-i\omega t} \tag{2.2}$$

Plugging this into the wave equation, we get,

$$\nabla^2 \boldsymbol{E} + k_o^2 \epsilon \boldsymbol{E} = 0 \tag{2.3}$$

where, $k_o = \frac{\omega}{c}$ [11]. For simplicity we assume that the wave is propagating only along the x-direction and there is no spatial variation along the y direction. The $z = 0$ plane coincides with the metal/dielectric interface and the dielectric profile is given as $\epsilon = \epsilon(z)$. The wave can be described by the following equation:

$$\boldsymbol{E}(x, y, z) = \boldsymbol{E}(z)e^{i\beta x} \tag{2.4}$$

where, β is the propagation constant [11]. Plugging this into Equation (2.3), we get the following equation:

$$\frac{\partial^2 \boldsymbol{E}(z)}{\partial z^2} + (k_o^2 \epsilon - \beta^2)\boldsymbol{E} = 0 \tag{2.5}$$

Different $\boldsymbol{E}$ and $\boldsymbol{H}$ components can be determined using Maxwell's curl equations. Since time dependence is harmonic, the wave is propagating in the x direction and there is no spatial variation along y direction, we get [11],

$$\frac{\partial E_y}{\partial z} = -i\omega\mu_o H_x \tag{2.6a}$$

$$\frac{\partial E_x}{\partial z} - i\beta E_z = i\omega\mu_o H_y \tag{2.6b}$$

$$i\beta E_y = i\omega\mu_o H_z \tag{2.6c}$$

$$\frac{\partial H_y}{\partial z} = i\omega\epsilon_o \epsilon E_x \tag{2.6d}$$

$$\frac{\partial H_x}{\partial z} - i\beta H_z = -i\omega\epsilon_o \epsilon E_x \tag{2.6e}$$

$$i\beta H_y = -i\omega\epsilon_o \epsilon E_z \tag{2.6f}$$

These equations have two sets of solutions. The first one is called transverse magnetic (TM) in which only E_z, E_x and H_y are non-zero. The second set is called transverse electric in which H_z, H_x and E_y are non-zero [11]. For TM modes, the Equations (2.6) reduce to:

$$E_x = -i\frac{1}{\omega\epsilon_o\epsilon}\frac{\partial H_y}{\partial z} \tag{2.7a}$$

$$E_z = -\frac{\beta}{\omega\epsilon_o\epsilon} H_y \tag{2.7b}$$

$$\frac{\partial^2 H_y}{\partial z^2} + (k_o^2 \epsilon - \beta^2) H_y = 0 \tag{2.7c}$$

For TE modes, the Equations (2.6) reduce to:

$$H_x = i\frac{1}{\omega\mu_o}\frac{\partial E_y}{\partial z} \tag{2.8a}$$

$$H_z = \frac{\beta}{\omega\mu_o} E_y \tag{2.8b}$$

$$\frac{\partial^2 E_y}{\partial z^2} + (k_o^2\epsilon - \beta^2)E_y = 0 \tag{2.8c}$$

Let us assume that the geometry consists of an interface between a conducting material for z < 0 described by a dielectric function $\epsilon_1(\omega)$ and a dielectric material for z > 0 with a purely real and positive dielectric constant ϵ_2. We look for wave solutions which are confined to the interface and decaying in the z direction. For TM modes, the solutions for z > 0 will be:

$$H_y(z) = A_2 e^{i\beta x} e^{-k_2 z} \tag{2.9a}$$

$$E_x(z) = iA_2 \frac{1}{\omega\epsilon_o\epsilon_2} k_2 e^{i\beta x} e^{-k_2 z} \tag{2.9b}$$

$$E_z(z) = -A_1 \frac{\beta}{\omega\epsilon_o\epsilon_2} e^{i\beta x} e^{-k_2 z} \tag{2.9c}$$

and for z < 0, the solutions will be:

$$H_y(z) = A_1 e^{i\beta x} e^{k_1 z} \tag{2.9d}$$

$$E_x(z) = -iA_1 \frac{1}{\omega\epsilon_o\epsilon_1} k_1 e^{i\beta x} e^{k_1 z} \tag{2.9e}$$

$$E_z(z) = -A_1 \frac{\beta}{\omega\epsilon_o\epsilon_1} e^{i\beta x} e^{k_1 z} \tag{2.9f}$$

where, k_1 and k_2 are components of the wave vector perpendicular to the interface. We note that for the wave solutions to be confined to the interface, the convention used in the exponents of Equations (2.9) require Re $[\epsilon_1] < 0$ and $\epsilon_2 > 0$. This condition is fulfilled at the dielectric-metal interface [11].

When metal nanoparticles are irradiated with electromagnetic radiation such that particle size is much less than the wavelength of the electromagnetic waves, the conduction electrons of the metal nanoparticles get displaced from their equilibrium position [3-6]. Consequently, a positive charge develops on the surface of the metal nanoparticles, which provides a restoring force to the electrons [3],[5-6]. The electrons are then pulled back to the surface. This phenomenon repeats and leads

to oscillation of the conduction electrons [3-6]. The quanta of these oscillations are called localised surface plasmons [5-6]. This is illustrated in Fig. 2.1.

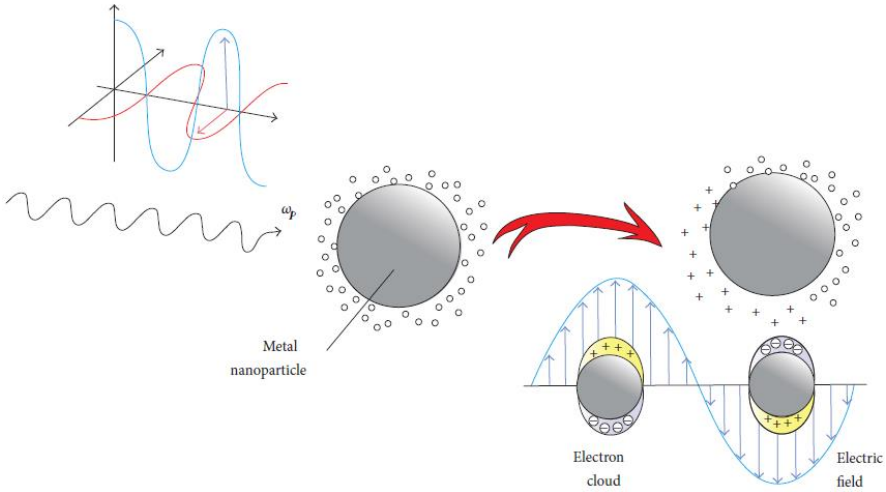

Figure 2.1: Localized Surface Plasmon Resonance [13].

Since we have electrons oscillating against fixed positively charged particles (nuclei), these oscillations produce dipoles [3],[5-6]. These dipoles produce an electric field near the surface of the particles, which is larger than the incident electric field [3],[5-6].

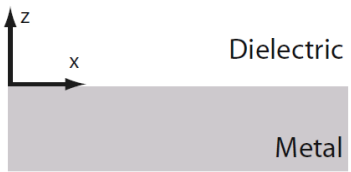

Figure 2.2: Dielectric-metal interface with the appropriate coordinate system [11]

At one particular wavelength called the resonance wavelength, all electrons oscillate coherently, leading to a dipole of maximum strength [3],[5-6]. Consequently, the near field (electric field enhancement) of these dipoles is maximum at this wavelength [5]. This phenomenon is termed as Localized Surface Plasmon Resonance [3],[6]. The reason behind resonance occurring at a particular wavelength can be understood by considering the mathematical analysis of this phenomenon [11]. Under quasi static approximation, the expression for polarizability of the dipole is [11]:

$$\alpha = 4\pi a^3 \frac{\epsilon - \epsilon_m}{\epsilon + 2\epsilon_m} \tag{2.10}$$

where $'a'$ is the particle radius, $'\epsilon'$ is the dielectric constant of the metal and ϵ_m is the dielectric constant of the surrounding dielectric. It can be seen that the

polarizability of the dipoles will be maximum when $\epsilon = -2\epsilon_m$. This is known as the Frohlich condition [11]. The wavelength at which this condition gets satisfied is called the resonance wavelength. If we monitor the electric field near the particles as a function of wavelength, then the electric field enhancement will manifest itself in the form of a narrow peak at a special wavelength, called the resonance wavelength. Some typical graphs we get are illustrated in Fig. 2.3 [12].

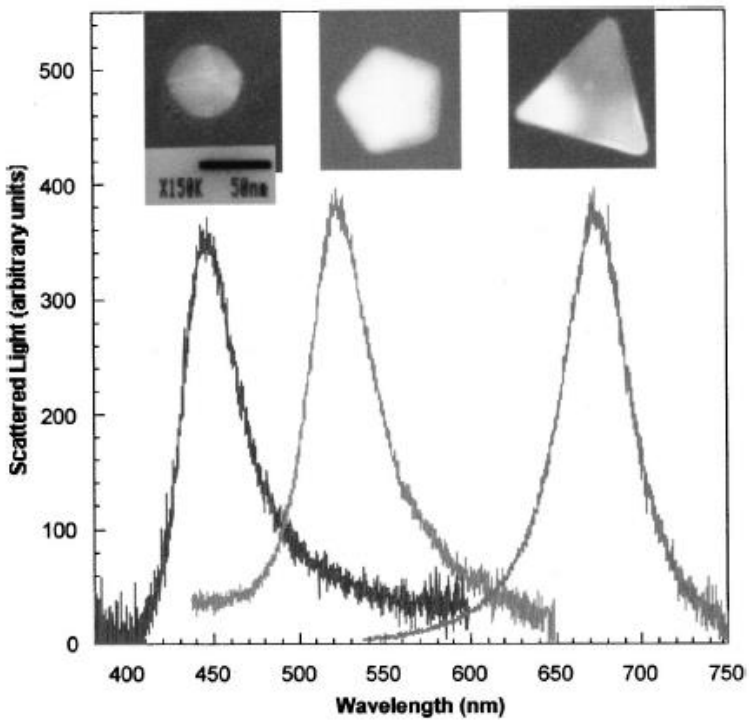

Figure 2.3: Measurements of scattered light by a spherical, pentagonal and a triangular nanoparticle. Inset shows the nanostructures under consideration. [12]

2.2 MATHEMATICAL PERSPECTIVE ON LOCALIZED SURFACE PLASMON RESONANCE

The phenomenon of Localized Surface Plasmon Resonance can be analyzed mathematically by considering a particle being irradiated by electromagnetic radiation such that size of the particle is much smaller than the wavelength of the incident radiation. This ensures that the phase of the oscillating electric field of the incident electromagnetic wave is constant over the entire particle surface. So, under quasi static approximation, the surrounding electric field can be assumed to be electrostatic in nature.

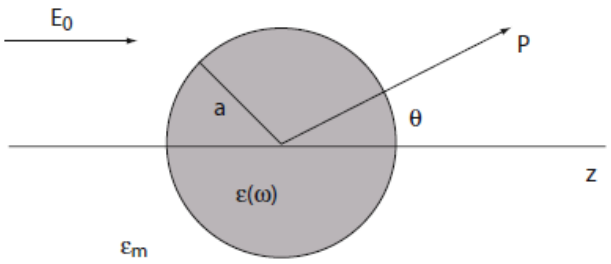

Figure 2.4: Geometry of the electrostatic problem [11].

The particle is assumed to have a spherical shape with a radius a and a dielectric response given by $\epsilon(\omega)$. The surrounding medium is assumed to have a dielectric constant ϵ_m. The electric field is given by E_o and is pointed in the z direction. Let the origin coincide with the centre of the sphere. Let the observation point P be a distance r away from the origin and at an angle θ with respect to the z axis. This is illustrated in the Fig. 2.4 [11].

We proceed by solving the Laplace equation. Due to spherical symmetry, the solution of the Laplace equation will be in the form of Legendre's polynomials of order l demonstrated by the following equation:

$$\phi(r,\theta) = \sum_{l=0}^{\infty} (A_l r^l + B_l r^{-(l+1)}) P_l \cos\theta \tag{2.11}$$

Since the solution has to be finite at origin, the constant $B_l = 0$ for potential inside the sphere. If we impose the boundary condition that tangential components of electric field are equal at $r = a$ and the electric field tends to $-E_o z$ as z tends to infinity, the expressions of potential comes out as [11]:

$$\phi_{in} = -\frac{3\,\epsilon_m}{\epsilon + \epsilon_m} E_o r \cos\theta \tag{2.12}$$

$$\phi_{out} = -E_o r \cos\theta + \frac{\epsilon - \epsilon_m}{\epsilon + 2\epsilon_m} E_o a^3 \frac{\cos\theta}{r^2} \tag{2.13}$$

It can be seen that potential outside the nanosphere seems to be a superposition of the incident field and field due to a dipole situated at particle centre. Hence, it can be concluded that the incident field induces a dipole moment inside the nanosphere. Thus, expression for potential outside the sphere can be written as [11]:

$$\phi_{out} = -E_o r \cos\theta + \frac{\boldsymbol{p}\,.\,\boldsymbol{r}}{4\,\pi\,\epsilon_o\,\epsilon_m\,r^3} \tag{2.14}$$

where **p** is the dipole moment and is defined as [11]:

$$\boldsymbol{p} = 4\,\pi\,\epsilon_o\,\epsilon_m\,a^3\,\frac{\epsilon - \epsilon_m}{\epsilon + 2\epsilon_m}\,\boldsymbol{E_o} \tag{2.15}$$

The dipole moment can be expressed in terms of polarizability 'α' as $\boldsymbol{p} = \epsilon_o\,\epsilon_m\,\alpha\,\boldsymbol{E_o}$, such that the expression of polarizability is given by [11]:

$$\alpha = 4\,\pi\,a^3\,\frac{\epsilon - \epsilon_m}{\epsilon + 2\epsilon_m} \tag{2.16}$$

It can clearly be seen that polarizability of the dipole inside the nanosphere experiences a maximum when $\epsilon + 2\epsilon_m$ is minimum. This implies:

$$Re[\epsilon(\omega)] = -2\epsilon_m \tag{2.17}$$

This is referred to as the Frohlich condition [11].

As the size of the particle increases such that the quasi static condition is no more satisfied, the electric field becomes more non-uniform over the particle surface. Hence, electrons start oscillating incoherently and out of phase. This effect of phase retardation manifests itself in the form of broadening of dipole resonance curve [3],[5]. The particle surface charge gets spread over a large area and hence, the surrounding medium better compensates the restoring force further slowing electron oscillations [3],[5].

The oscillating electrons produce polarization in opposite direction in the surrounding dielectric, reducing the restoring force [3],[5]. This altered restoring force manifests itself in the form of a red shift in wavelength at which the resonance occurs [3],[5-6],[11]. This can be understood in yet another way. A change in dielectric constant of the medium brings about a change in the wavelength at which the Frohlich condition gets satisfied [3],[11]. This is illustrated in Fig. 2.5.

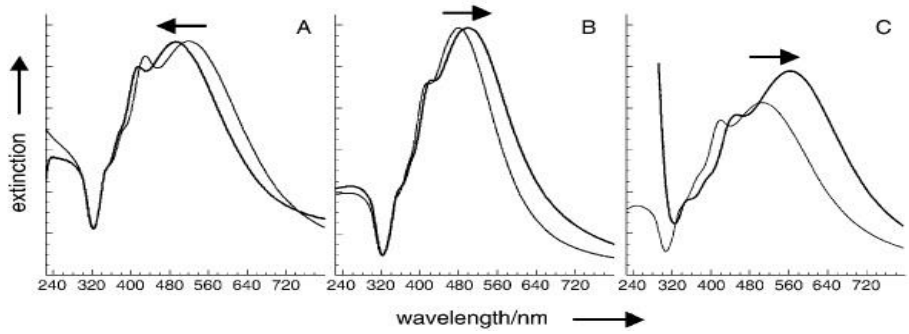

Figure 2.5: Shift in the resonance wavelength as the dielectric environment is changed from a) Isopropanol to Teflon b) water to silica c) water to titania [3].

Additionally, interband transitions damp the oscillations as well [3]. Since the energy of the incident electromagnetic radiation gets used in interband

transitions, it leads to lower field enhancement [3]. The energy required to bring about interband transitions overlaps with the energy required to bring about SPR [3].

2.3 VARIOUS APPLICATIONS OF SURFACE PLASMON RESONANCE AND LOCALIZED SURFACE PLASMON RESONANCE

2.3.1 Photovoltaics

Photovoltaics is the discipline that deals with the conversion of solar energy into electricity [14]. Current technology makes the use of thick Silicon wafers (thickness of around 180 – 300 microns) and the main cost of production comprises of the silicon material and processing [14]. So, in order to make solar energy economically feasible and competent with fossil fuel energy, thin Silicon wafers (with a thickness of around 1- 2 microns) have been introduced [14]. These, however, suffer from a disadvantage. They have lower absorbance for a large part of the solar spectrum as shown in Fig. 2.6a.

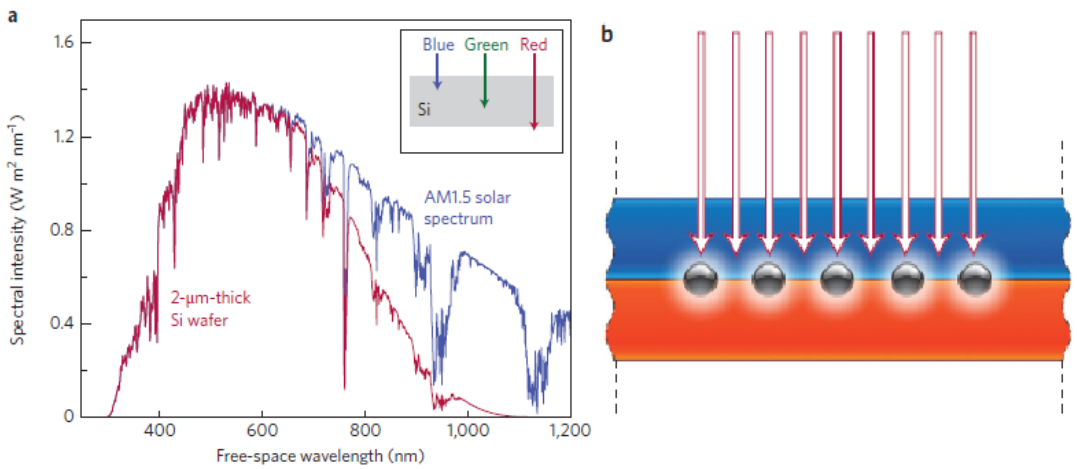

Figure 2.6: (a) Red curve indicates the absorbance of the thin solar cell. Blue curve indicates the solar spectrum. (b) Light trapping by excitation of localized surface plasmons on the surface of metal nanoparticles [14].

As can be seen from Fig. 2.6a, thin silicon wafer poorly absorbs the solar spectrum especially in the wavelength range of 600 – 1100 microns.

Light trapping in thick silicon wafers, is generally done with the help of structures involving surface textures [15-16]. These large-scale geometries, however, cannot be used in thin silicon wafers because of geometrical reasons [14]. So, one

solution is to embed metal nanoparticles in the thin silicon wafers as shown in Fig. 2.6b.

Due to excitation of localized surface plasmons, electric field gets enhanced near the surface of the particles leading to the generation of a larger number of electron-hole pairs.

2.3.2 SP based biosensor

The dependence of the resonance wavelength of the Surface Plasmon Resonances on the dielectric environment can help us develop biosensors. Haes et. al., in 2004, reported one such application where they designed a biosensor to detect Alzheimer's disease [17]. They used silver nanotriangles [17]. Their design and results are shown in Fig. 2.7.

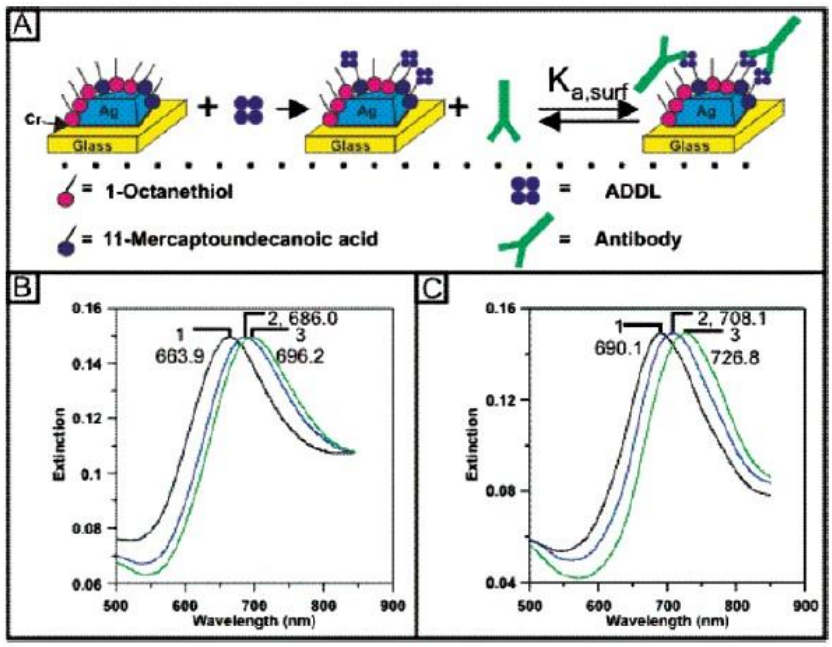

Figure 2.7: Surface Plasmon based biosensor [17].

On the surface of the nanotriangles, they deposited a layer of self-assembled monolayer (SAM) of 1:3 11-mercaptoundecanoic acid (11-MUA, Aldrich))/1-octanethiol (1-OT, Aldrich) [17]. ADDL molecules, which cause neurological dysfunction in Alzheimer's disease, were then made to bind with the SAM layer on the nano-triangles. A redshift of 22.1 nm in the resonance wavelength was observed [17]. Then, anti-ADDL molecules, the antibody which is produced by the human body to fight ADDL, was allowed to bind with the ADDL molecules. A

redshift of 10.2 nm was observed [17]. This experiment was repeated by using a different concentration of anti-ADDL and the corresponding redshift was observed to be 18.7 nm [17].

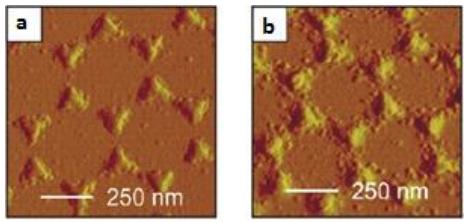

Figure 2.8: AFM images showing nano-triangles (a) before and (b) after the binding of anti-ADDL [17].

Fig. 2.8 shows the AFM images of the nano-triangles before and after anti-ADDL bonding.

2.3.3 Surface Plasmon based H_2O_2 sensor

Vasileva et. al., in 2010, designed a Surface Plasmon based H_2O_2 sensor [18]. Determination of Hydrogen peroxide is important because H_2O_2 is a major product in reactions where oxidase enzymes are used as a catalyst. Other important fields where H_2O_2 is used extensively, include – food, pharmaceutical and clinical laboratory. H_2O_2 sensors developed until now are unstable and hard to reproduce. Surface Plasmon based H_2O_2 sensors provide a better alternative.

They prepared Ag-nanoparticle dispersion by reduction of $AgNO_3$using a reducing agent, a capping agent and a catalyst [18]. Then they introduced a 0.001 mol/L solution of H_2O_2 in the nanoparticle dispersion [18]. A redshift from 408 nm to 417 nm is seen in the resonance wavelength [18]. This is illustrated in Fig. 2.9.

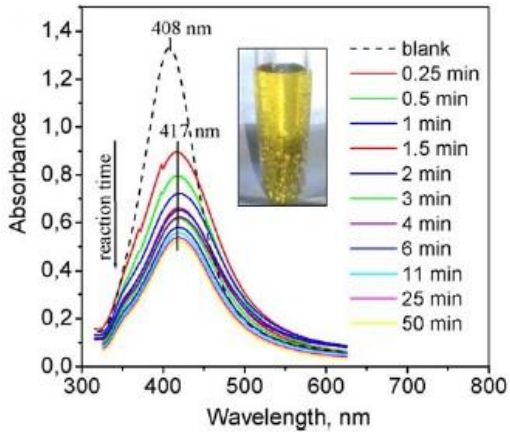

Figure 2.9: Redshift of 9 nm in the resonance wavelength. Inset shows bubbles that are generated when H_2O_2 reacts with Ag-nanoparticles [18].

2.3.4 Surface Plasmon based heavy metal ion detector

In 2014, Verma *et al.* proposed a Surface Plasmon Resonance based fiber optic sensor for the detection of heavy metal ions in contaminated water [19]. They deposited a layer of silver nanoparticles on a small unclad portion of the optical fiber [19]. This layer of silver nanoparticles was then coated with Indium Tin Oxide in order to improve the sensitivity of the sensor [19]. An additional coating of chitosan and conducting polymer was applied on top [19]. This improves the binding of heavy metal ions with silver nanoparticles [19].

They observed the transmitted power after exposing the sensor with different concentrations of heavy metal ions. The results they obtained are shown in Fig. 2.10.

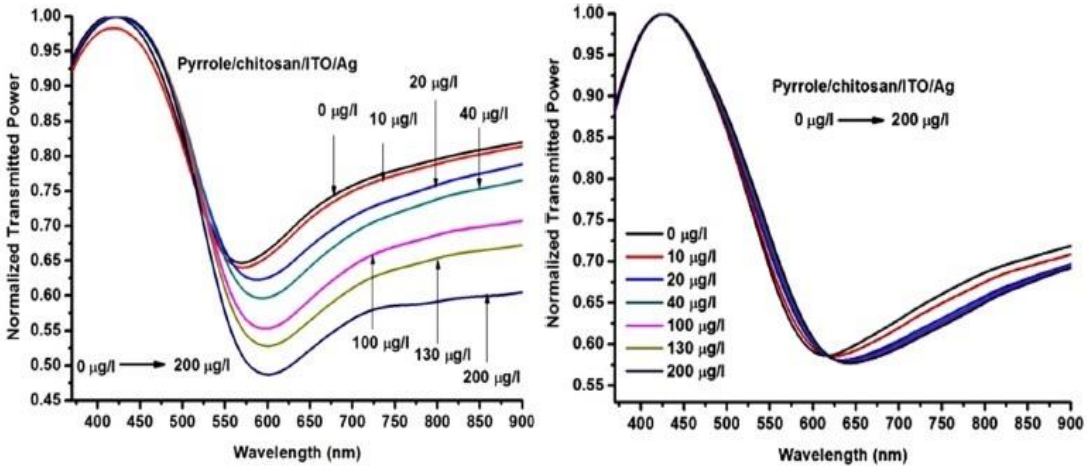

Figure 2.10: Redshift in resonance wavelength in case of cadmium ions (left) and lead ions (right) [19].

Surface Plasmon Resonance finds use in many other applications such as optical waveguides [20-22], plasmonic switches [23], OTA sensor [24], LED [25] and plasmonic lasers [26-27].

2.3.5 Plasmonic enhancement structures

The radiative electromagnetic field, which results from oscillation of electrons on the surface of metal nanoparticles (upon incident optical radiation), contain a broad range of frequencies. This electromagnetic radiation or photoluminescence can be of two types: Single photon luminescence (SPPL) and multi-photon luminescence (MPPL) [28]. Single photon and multi-photon broadband

emissions are quite different from each other [28]. SPPL increases with decreasing wavelength leading to a peak [28]. MPPL decreases with decreasing wavelength and hence the peak is absent [28]. Due to the *photoluminescence* produced by metal nanoparticles, they can be employed as optical radiator (antenna) [28].

Photoluminescence can also be categorised based on the specific range of electromagnetic spectrum emitted by *nano-antennas.* Visible photoluminescence, for example, can be seen in smooth metal films as well as noble metal nanostructures [29]. In smooth metal films, visible photoluminescence is majorly due to inter-band transitions, with little contributions of LSPR, and in metal nanostructures, it is majorly due to LSPR [29]. Infrared photoluminescence, on the other hand, majorly occurs in noble metal nanostructures [29].

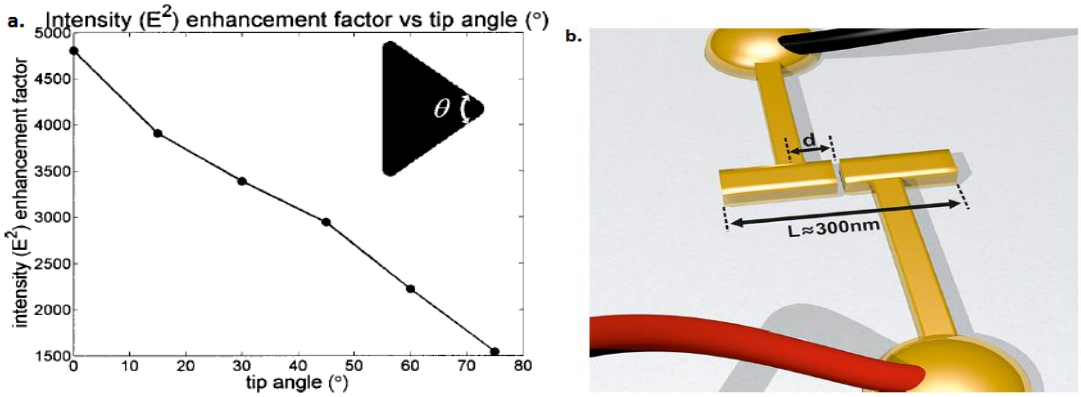

Figure 2.11: (a) Intensity enhancement as a function of tip angle [32]. (b) Proposed design. Distance between the centre of the feed and centre of the lead is denoted by 'd'. 'L' is the total length of the antenna [34].

Researchers, throughout the world, have analysed different geometries in an attempt to find the one with best characteristics. In 2005, Schuck *et al.* experimentally determined the photoluminescence intensity enhancement factor relative to the incident light, for bowtie shaped nano-antennas [30]. Bowtie shaped nano-antennas consist of two metallic triangles, facing tip to tip [30]. They did this experiment for structures of length ~ 75nm and central gap of 20 nm (where plasmon coupling between the triangles is prominent) [30]. They observed an intensity enhancement factor over 1500 [30]. They also repeated the experiment with central gap of 400 nm and found that plasmon coupling was minimal [30]. So much so, that each triangle, constituting a bowtie structure, acted like an isolated nanoparticle [30]. These values were in good agreement with their FDTD simulation results which they have reported in a different article [31]. In 2003, Crozier *et al.*, determined the

influence of shape, size and material of antenna on the intensity enhancement and resonance wavelength [32]. Their result for intensity enhancement as a function of tip angle of the bowtie structure is shown in Fig. 2.11a.

In 2005, Eisler *et al.*, experimentally demonstrated that linear dipole nano-antennas can be matched at optical wavelengths [33]. They fabricated gold dipoles with lengths varying from 190 to 400 nm with a feed gap of 20 nm and 45 nm width [33]. A laser source with operating frequency of 830 nm was used [33]. The spectrum observed was due to two phenomena: Two-Photon Photoluminescence (TPPL) as well as White Light Super Continuum generation (WLSC) [33]. They observed something very peculiar about optical antennas. As per Electromagnetic theory, the half wavelength dipole length should be 415nm. However, a maximum emission was achieved at 255 nm demonstrating that simple downscaling of microwave antennas in the optical regime is not possible [33]. This is due to the occurrence of plasmon modes leading to large electric field enhancement in the feed gap [33].

Optical antennas can also be realised using a new class of devices called electro plasmonic devices. These are called electrically connected optical antennas. For a device to be electro plasmonic, it must fulfil three conditions. First, it should contain plasmonic properties which can support resonantly enhanced electric fields [34]. Second, it can support large DC fields, just like the field between the two plates of a parallel plate capacitor [34]. Third, a spatial overlap between the two kinds of field should exist [34]. Prangsma *et al.*, in 2012, proposed design of electrically driven optical antennas, consisting of two-wire antennas with a feed gap between them [34]. This design is given in Fig. 2.11b.

Since the resonance characteristics are extremely sensitive to the environment of the antenna, they first determined the optimum position of the metal contacts for the wires using FDTD simulations [34]. Then they fabricated the design and determined the resonance characteristics for four different lengths of the antennas and resistance of the gap by applying a voltage (0-10V) across the two wires [34]. Their results are shown in Fig. 2.12a. The resistance of the antennas came out to be about 3 gigaohms [34].

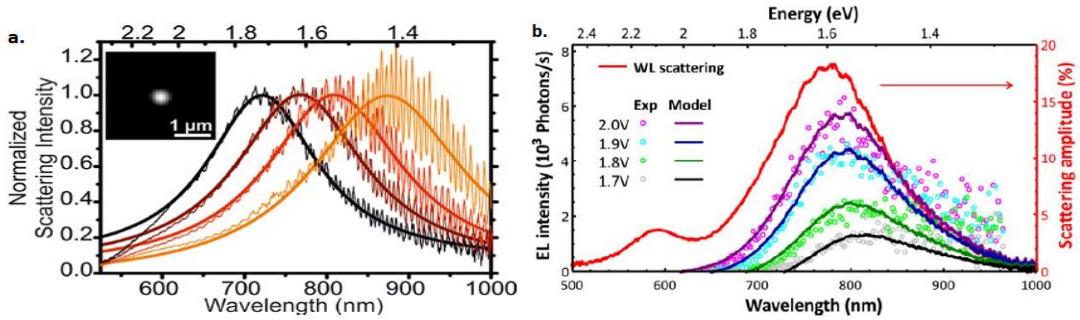

Figure 2.12: (a) The scattering spectra of 380 nm (yellow), 340 nm (red), 310 nm (dark red) and 280 nm (black) long antennas [34]. (b) Electroluminescence spectra for the electrically driven optical antenna for different applied voltages [35].

In 2015, J. Kern *et al.* designed an electrically driven optical antenna with a nanoparticle in the feed gap of the antenna to produce a lateral tunnel junction [35]. This leads to tunnelling of electrons or 'quantum shot noise' resulting in current fluctuations at optical frequencies [35]. Fig. 2.12b shows the plot of the obtained spectra against the wavelength for different applied voltages [35].

In 2006, Cubukcu *et al.*, demonstrated the use of optical antennas in order to generate high intensity optical fields from laser diodes [36]. They termed this as plasmonic laser antennas [36]. Conventionally, the light coming out from a laser is made to pass from a sub-wavelength aperture in order to get high intensity optical fields. The resulting spot size is of the order of tens of nanometres [36]. The optical fields generated using this method, however, have low power (throughput) [36]. This is because, the power decays as the fourth power of the diameter of the aperture [36]. The authors overcome this drawback by making use of plasmonic coupled nanoparticles instead of sub-wavelength apertures [36]. They integrated a pair of gold nanorods on one of facets of the diode laser [36]. The nanorods were 130 nm long, 50 nm wide, 50 nm thick and separated by a distance of about 30 nm from each other [36]. Since, optical antennas are now being employed instead of apertures, the output power no longer experiences decay [36]. Their results are shown in Fig. 2.13**.**

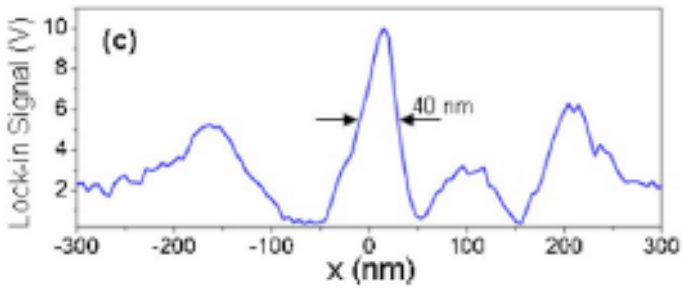

Figure 2.13: Electric field distribution along the axis of the antenna [36].

They further proposed a better design consisting of bowtie shaped nanoparticles instead of nanorods [36]. This could eliminate the multiple peaks present in the output spectra shown in Fig. 2.13 [36].

In 2006, Hecht *et al.*, demonstrated the use of optical antennas in spectroscopic characterization of nanostructures [37]. By taking an example of a dipole antenna, they showed that the spatial resolution achieved by the near field optical microscopy is of the order of the width of the feed gap of the optical antenna [37].

According to classical antenna theory, the length of antenna is directly proportional to the wavelength of the incident (or transmission) radiation. This is mathematically represented as L=const x lambda. The half wave dipole antenna, for example, has L= (1/2) x lambda. This relation, however, is no longer valid at optical frequencies as the length of the antennas is so small that light does not perfectly reflect from the metal surface, but, penetrates the metal and induces collective oscillations of the conduction of electrons in the metal [38]. Hence, at optical frequencies, an antenna does not respond to the actual incident radiation, but to a different effective wavelength [38]. In 2007, Novotny, derived the effective wavelength which is given as:

$$\lambda_{eff} = n_1 + n_2(\lambda/\lambda_p) \tag{2.18}$$

where, λ_p is the plasma wavelength and n_1 and n_2 are coefficients that depend upon the antenna geometry and dielectric properties of the metal [38]. He arrived at this relation assuming the metal is made up of linear segments with radius much less than wavelength of the incident radiation and the metal can be characterised by a free electron gas under the Drude model [38].

Alaverdyan *et al.*, in 2007, studied the coupling effects of chains of nanoholes embedded in thin gold films [39]. They showed that spectral response of the nanoholes could be tuned by exploiting the interaction between the surface plasmon resonances of individual nanoholes [39]. The tuning of the spectral response is achieved due to the superposition of the far field of the individual nanoholes [39].

Until now, most of the research articles related to optical antennas address the feeding element only without paying much attention to the feeding strategy. Li *et al.*, proposed an optical antenna along with feeding mechanism [40].

Their design consists of a cylindrical nanowire, made up of a dielectric coated with silver, placed near a slab waveguide [40]. Their design is shown in Fig. 2.14**.**

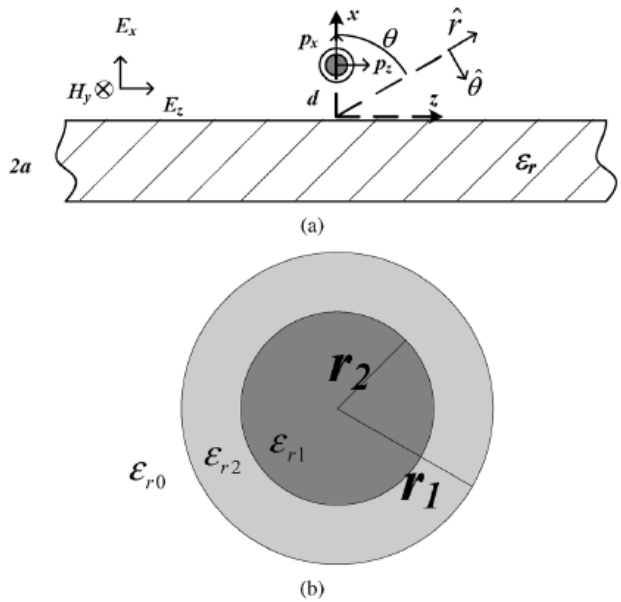

Figure 2.14: (a) Nanowire kept in the vicinity of slab waveguide. (b) Nanowire consists of a dielectric of radius r_2 coated with silver with outer radius being r_1 [40].

The nanowire interacts with the TM wave travelling inside the waveguide and scatters optical waves acting as a radiator [40]. Reciprocally, a plane wave incident on the nanowire can cause TM modes to be coupled to the waveguide, acting as a receiver [40]. They have calculated the polarizability of the cylindrical nanowire using Mie scattering theory [40]. Additionally, they have performed theoretical analysis and numerical simulations (based on Finite Element method) of the system [40].

2.4 Hybridization Model for Nanoshells and other Complex Nanoparticles

In 2003, Prodan *et al.* described the plasmon response of complex nanoparticles through an intuitive picture [41]. According to their description, the plasmon response of a nanoshell can be understood by considering plasmons induced on the dielectric-metal interface inside the cavity and plasmons induced on the dielectric-metal interface at the outer surface of the nanoshell (Fig. 2.15a) [41]. These two plasmons interact or "hybridize" to form a symmetric (bonding) configuration and an anti-symmetric (anti-bonding) configuration [41].

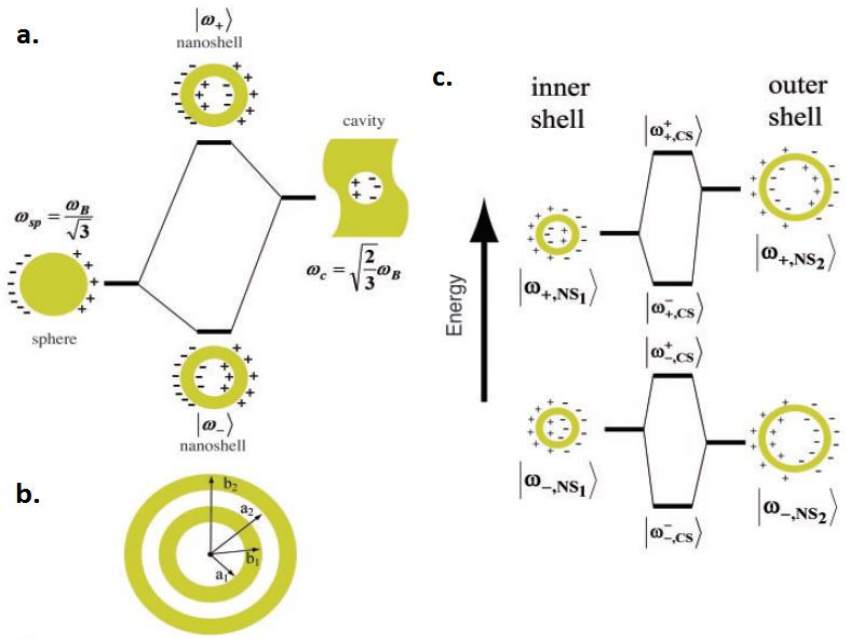

Figure 2.15: (a) Energy level diagram depicting hybridization between plasmons inside the cavity and on the surface on the nanoshell. (b) Geometry depicting the four-layer concentric nanoshell. (c) Energy level diagrams depicting hybridization [41].

For a four-layer concentric nanoshell shown in Fig. 2.15b [41], the outer shell and inner shell, each can form both antibonding and bonding plasmonic modes giving rise to four hybridized plasmonic modes as shown in the Fig. 2.15c [41]. The thickness of the dielectric spacer layer determines the strength of interaction of the plasmonic modes of the inner shell and outer shell [41]. So, the plasmonic response can be tuned using the spacing between the two interacting plasmon surfaces and material of the metal itself.

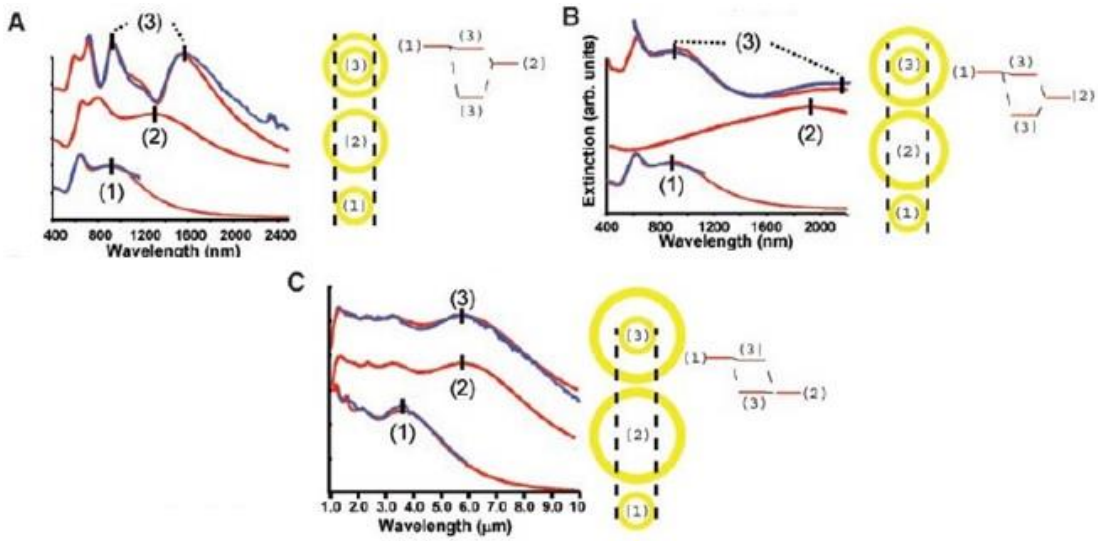

Figure 2.16: (a) Strong coupling between inner and outer nanoshell. (b) Weak coupling between inner and outer nanoshell. (c) No coupling between inner and outer nanoshell [41].

Three types of 4-layer nanoshells were discussed theoretically (figure 27) [41]. The first one has a small dielectric layer thickness (Fig. 2.16a) [41]. This nanoshell experiences strong interactions and hence the response of the nanoshell is different from the response of the two isolated shells. The shape of the spectral response shows that it is antisymmetric [41]. Fig. 2.16b depicts the nanoshell with weak interactions [41]. As the interactions are weak, the response of the 4-layer shell is almost same the same as the response of isolated shells with only a small difference. Fig. 2.16c depicts no coupling [41]. Since there is no coupling; the curve is the same as that of one of the isolated shells.

CHAPTER 3

FINITE DIFFERENCE TIME DOMAIN – THE NUMERICAL SIMULATION TOOL

The modelling of the various nanostructures discussed in this thesis are based on the technique of Finite Difference Time Domain (FDTD) method. This involves, dividing the simulation region into 'cells' followed by solving the finite difference approximation of the scalar wave equation at each node of all the cells [42]. It then repeats this step for successive 'time steps' [42].

3.1 YEE'S ALGORITHM

In 1966, Yee gave an algorithm which solves the electric and magnetic field simultaneously (rather than solving for electric or magnetic field alone) in both, space and time [42]. The algorithm solves the Maxwell's curl equations in 3D. This algorithm splits or grids the three dimensional space into *Yee cells* [42]. Each Yee cell consists of four magnetic field components circulating (or curling) one electric field component and four electric field components circulating one magnetic field component as shown in Fig. 3.1a.

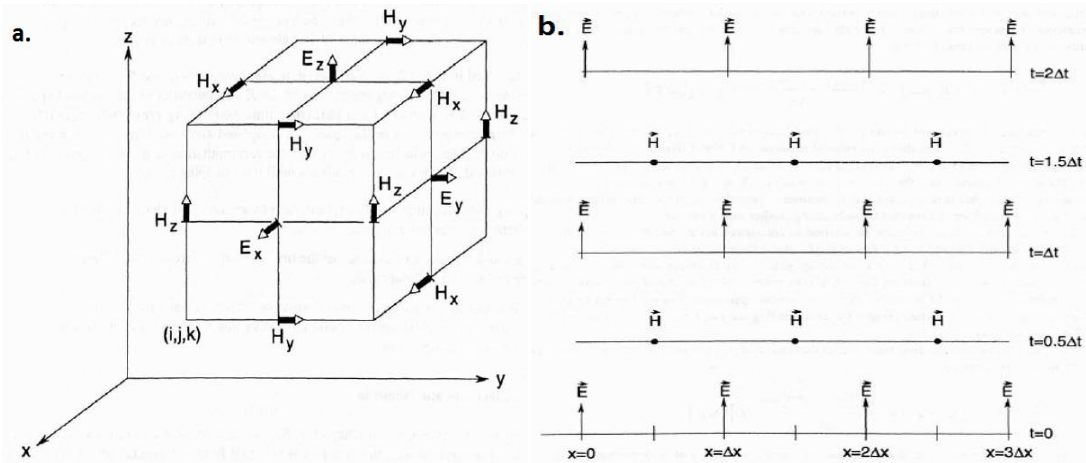

Figure 3.1: (a) Yee cells, (b) Leapfrog arrangement in time [42].

The Yee algorithm, first, determines the electric field components along the entire space for a particular time step, based on the values of magnetic field

components stored in memory at the previous time step. It then determines the magnetic field components through the electric field components. Therefore, the Yee algorithm implements a *leapfrog* arrangement in time [42]. This is illustrated in Fig. 3.1b.

The notation used to represent a lattice point is as follows [42]:

$$(i, j, k) = (i\,\Delta x, j\,\Delta y, k\,\Delta z) \tag{3.1}$$

where, Δx, Δy and Δz denote the step size in the x, y and z direction and i, j and k denote the index of the particular lattice point.

Notation used to represent any function of time and space is as follows [42]:

$$u\,(i\,\Delta x, j\,\Delta y, k\,\Delta z) = u^{n}_{i,j,k} \tag{3.2}$$

where, Δt denotes the time step and n is another integer.

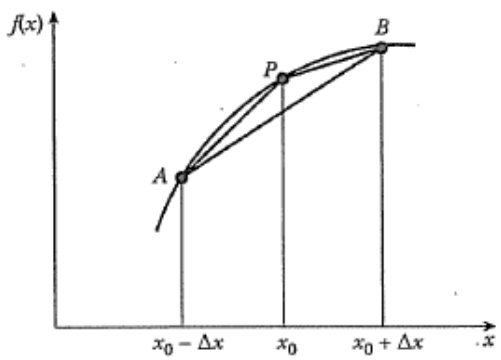

Figure 3.2: Function f(x) and its derivatives [43].

The derivative, tangent at point P or slope of the function $f(x)$ shown in figure 3.2**,** can be approximated using slope of the arc PB:

$$f'(x_o) \cong \frac{f(x + x_o) - f(x_o)}{\Delta x} \tag{3.3}$$

This is the forward-difference formula [43]. We can also use the slope of arc AP to get a backward-difference formula [43]:

$$f'(x_o) \cong \frac{f(x_o) - f(x - x_o)}{\Delta x} \tag{3.4}$$

We can also get a central difference equation using the slope of arc AB [43]:

$$f'(x_o) \cong \frac{f(x + x_o) - f(x - x_o)}{2\Delta x} \tag{3.5}$$

Using the Equations (3.1), (3.2) and (3.5), Yee calculated the partial first derivative of u with respect to x and t:

$$\frac{\partial u}{\partial x}(i\Delta x, j\Delta y, k\Delta z, n\Delta t) = \frac{u^{n}_{i+1/2,j,k} - u^{n}_{i-1/2,j,k}}{\Delta x} + O[(\Delta x)^2] \tag{3.6}$$

$$\frac{\partial u}{\partial t}(i\Delta x, j\Delta y, k\Delta z, n\Delta t) = \frac{u^{n+1/2}_{i,j,k} - u^{n-1/2}_{i,j,k}}{\Delta t} + O[(\Delta t)^2] \tag{3.7}$$

It can be observed that Yee used a step of $\Delta x/2$ on either side of the observation point instead of a full Δx. This ensures the proper interleaving of E and H components in time. For example, a step of Δx between two adjacent E components, which are located a distance $\Delta x/2$ on either side of an H component would be used to compute $\partial E/\partial x$ and allow stepping of H component in time [42]. Hence, this helps us realise the leapfrog arrangement. These equations were used to determine a numerical approximation of the Maxwell's curl equations. The field component E_x is given as [42]:

$$\begin{aligned} & E_x\big|^{n+1/2}_{i,j+1/2,k+1/2} \\ &= \left(\frac{1 - \frac{\sigma_{i,j+1/2,k+1/2}\,\Delta t}{2\,\epsilon_{i,j+1/2,k+1/2}}}{1 + \frac{\sigma_{i,j+1/2,k+1/2}\,\Delta t}{2\,\epsilon_{i,j+1/2,k+1/2}}}\right) E_x\big|^{n-1/2}_{i,j+1/2,k+1/2} \\ &+ \left(\frac{\frac{\Delta t}{\epsilon_{i,j+1/2,k+1/2}}}{1 + \frac{\sigma_{i,j+1/2,k+1/2}\,\Delta t}{2\,\epsilon_{i,j+1/2,k+1/2}}}\right)\left(\frac{H_z\big|^{n}_{i,j+1,k+1/2} - H_z\big|^{n}_{i,j,k+1/2}}{\Delta y}\right. \\ &\left. - \frac{H_y\big|^{n}_{i,j+1/2,k+1} - H_y\big|^{n}_{i,j+1/2,k}}{\Delta z} - J_{source_x}\big|^{n}_{i,j+1/2,k+1/2}\right) \end{aligned} \tag{3.8}$$

and the H_y component is determined to be [37]:

$$\begin{aligned} & H_y\big|^{n+1}_{i,j+1/2,k+1} \\ &= \left(\frac{1 - \frac{\sigma^{*}_{i,j+1/2,k+1}\,\Delta t}{2\,\mu_{i,j+1/2,k+1}}}{1 + \frac{\sigma^{*}_{i,j+1/2,k+1}\,\Delta t}{2\,\mu_{i,j+1/2,k+1}}}\right) H_y\big|^{n}_{i,j+1/2,k+1} \\ &+ \left(\frac{\frac{\Delta t}{\mu_{i,j+1/2,k+1}}}{1 + \frac{\sigma^{*}_{i,j+1/2,k+1}\,\Delta t}{2\,\mu_{i,j+1/2,k+1}}}\right)\left(\frac{E_z\big|^{n+1/2}_{i+1/2,j+1/2,k+1} - E_z\big|^{n+1/2}_{i-1/2,j+1/2,k+1}}{\Delta x}\right. \\ &\left. - \frac{E_x\big|^{n+1/2}_{i,j+1/2,k+3/2} - E_x\big|^{n+1/2}_{i,j+1/2,k+1/2}}{\Delta z} - M_{source_y}\big|^{n+1/2}_{i,j+1/2,k+1}\right) \end{aligned} \tag{3.9}$$

where, σ is the electrical conductivity, $\sigma^*$is the equivalent magnetic loss, ϵ is the electrical permittivity, μ is the magnetic permeability, J_{source} is the electric current density due to source and M_{source} is the magnetic permeability due to source. Similarly, based on Yee's algorithm, we can also derive equations for field components E_y, E_z, H_x and H_z. These are the numerical approximations that form the basis of the FDTD method.

3.2 MAGIC TIME STEP

If we put $c\,\Delta t = \Delta x$, then we get an exact solution of the scalar wave finite difference equation [42]. The approximations due to Taylor series expansion are also cancelled by using this condition. This condition is known as the magic time step [42]. For the solution to be numerically stable, we generally use $c\,\Delta t \leq \Delta x$ [42].

3.3 PERFECTLY MATCHED LAYER BOUNDARY CONDITIONS

Perfectly Matched Layer (PML) absorbing boundary conditions are used to terminate the boundaries of a FDTD simulation region [42]. They have the same physical effect as anechoic chambers. PML layers absorb the incoming electromagnetic waves regardless of frequency, polarization and incident angle [42]. Consequently, PML act as a reflectionless, highly absorbing material. PML boundaries can be used to terminate even non-linear, inhomogeneous and anisotropic media [42].

PML was first introduced by Berengor in 1994 [42]. He derived the split field PML, wherein, vector field components were split into two orthogonal components [37]. In subsequent years, many modifications were introduced, such as stretched-coordinate PML, convolutional PML and uniaxial PML [42].

CHAPTER 4

TUNABILITY OF EM ENHANCEMENT AND RESONANCE WAVELENGTH IN BIMETALLIC NANOPARTICLE DIMERS

High electromagnetic enhancement can be used to develop refractive sensors [17-19], optical waveguides [20-22], improve the efficiency of solar cells [14], etc. It is known that when metallic nanoparticles are brought in close proximity (spacing <20 nm), high electromagnetic hotspots are created due to the excitation of coupled plasmons [11]. If the shapes, sizes, materials and proximity of these nanoparticles are well engineered, yet higher electromagnetic fields can be created on illumination with light of resonant wavelength. In this chapter, we explore the optimization of these dimensional and shape aspects of metallic nanoparticle dimers to understand the electromagnetism behind this enhancement. Furthermore, we demonstrate through an exhaustive set of simulations that these substrates can exhibit passive tunability of the resonance wavelength which makes these substrates suitable to be employed with different laser sources.

4.1 SUMMARY

It is well known that two nanospheres, when illuminated with the light of the right wavelength, and when placed in close proximity of each other, give rise to coupled plasmon resonances leading to high electromagnetic enhancement in the EM hotspot between them. Hence, two gold nanospheres of radius of 40 nm, separated by a distance of 20 nm, were simulated in order to observe their plasmonic properties. The inter-particle distance and the number of particles were varied. Bimetallic nanospheres consisting of a silver core coated with gold were then simulated. A blue-shift of 10 nm was observed in the resonance wavelength, indicating the prospect of passive tunability.

4.2 DIMERS OF GOLD NANOPARTICLES

Out of all the possible geometries, metal nanospheres are the simplest and easiest to fabricate. Two gold nanospheres, when placed sufficiently close to each other, would allow a high electromagnetic enhancement. The schematic consists of two gold nanoparticles, separated by a distance of 20 nm, being irradiated with electromagnetic radiation of wavelength ranging from 0.4 microns to 1.1 microns. The radius of each particle was taken to be 40 nm. If the radius of the nanoparticle is taken to be about 80 nm, the quasi-static approximation would fail, leading to Mie scattering. For radius of about 20 nm and less, the polarizability of the nanoparticle would be very low due to small size, leading to low EM enhancement. Hence, 40 nm is an optimum size to begin with.

The particles were surrounded by 'Perfectly Matched Layer' boundaries. These boundaries absorb all the radiation that is incident upon them and hence simulates an 'isolated system'. The schematic is illustrated in Fig. 4.1.

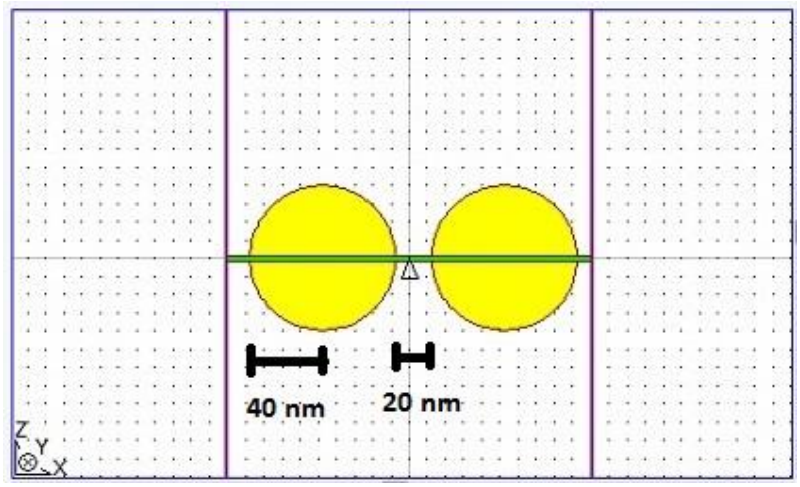

Figure 4.1: Two gold nanoparticles separated by a distance of 20 nm.

4.3 RESULTS AND DISCUSSIONS

4.3.1 Dimer of gold nanoparticles with inter-particle distance of 20 nm.

For the schematic described in section 4.2, the graph of electric field intensity as a function of wavelength that was obtained is shown in Fig. 4.2.

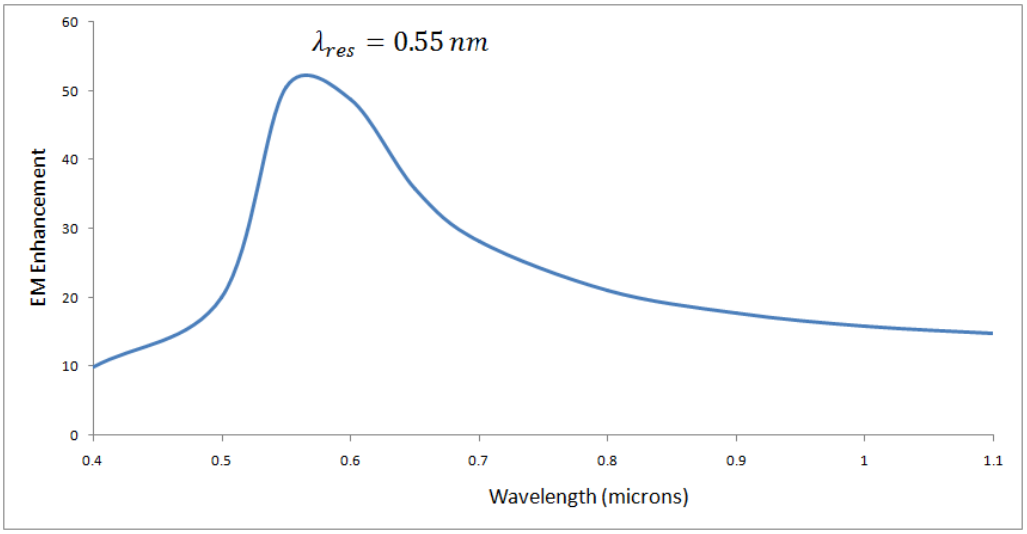

Figure 4.2: EM Enhancement vs wavelength for a dimer of gold nanospheres having a radius of 40 nm and separated by a distance of 20 nm.

As can be seen from the graph, the electric field intensity due to the excitation of Surface Plasmons in gold nanoparticles is 50 times more than the incident field (at the resonance wavelength).

4.3.2 Varying the inter-particle distance

These simulations were run with different values of inter-particle distance. The results for inter-particle distance of 11 nm and 5 nm are shown in Fig. 4.3.

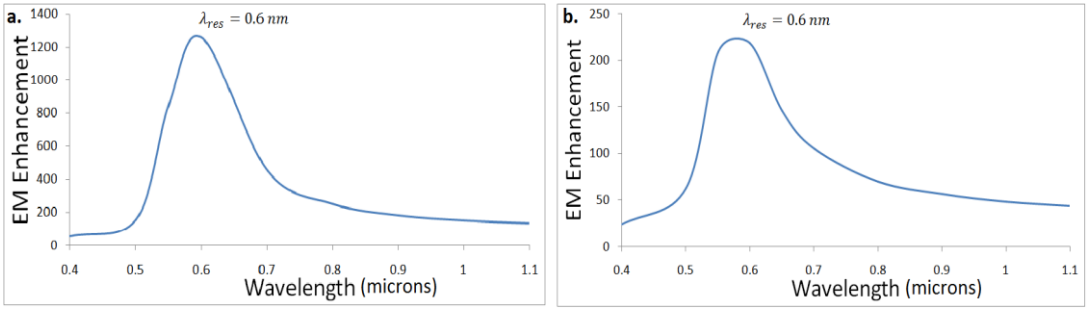

Figure 4.3: EM Enhancement vs wavelength of gold nanospheres for an inter-particle spacing of (a) 5 nm and (b) 11 nm when the radius is 40 nm.

The graph illustrating the comparison between these three results is shown in Fig. 4.4. It is clear from Fig. 4.4 that the electric field enhancement increases with decreasing inter-particle spacing. This is due to the fact that when we have more than one particle, the electric field produced due to oscillating electrons of the adjacent particles overlap. At one particular wavelength (resonance wavelength), the fields due to adjacent particles constructively interfere, producing a sharp rise in the field enhancement. Thus, at the resonance wavelength, conduction electrons of

both the particles, put together, oscillate coherently and in phase with respect to each other.

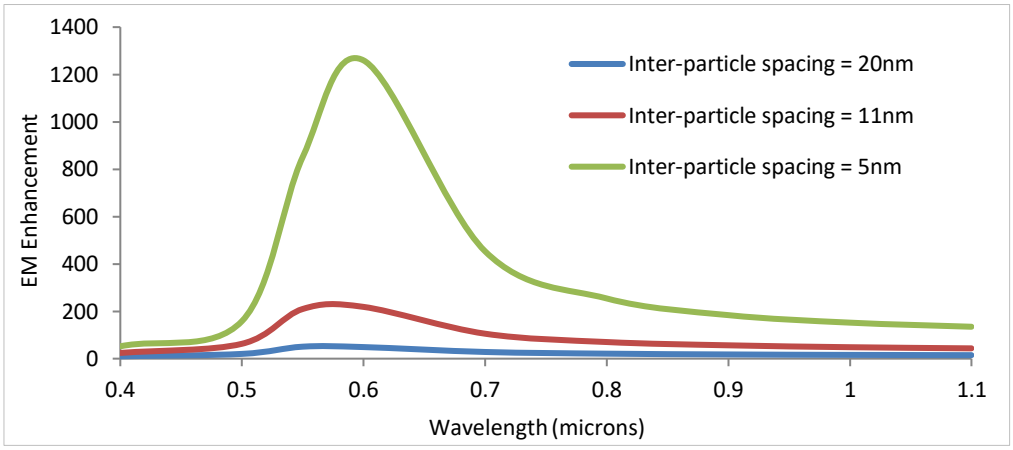

Figure 4.4: Comparison between EM Enhancement for a dimer of gold nanospheres for inter-particle spacings of 20 nm, 11 nm and 5 nm when the radius is 40 nm.

This particular property can be exploited in the field of photovoltaics. As mentioned in section 2.3.1, the efficiency of solar cells depends upon the electron-hole pair generation in the depletion region of the semiconductor [14]. The generation of electron-hole pairs can be greatly improved by embedding metal nanoparticles in this region [14]. This process of generation of carriers can be optimized by choosing an appropriate inter-particle spacing. Due to enhanced electric field near the surface of the metal nanoparticles, the light will be more effectively coupled to the depletion region leading to the generation of more electron-hole pairs [14].

4.3.3 An Array of Gold nanoparticles

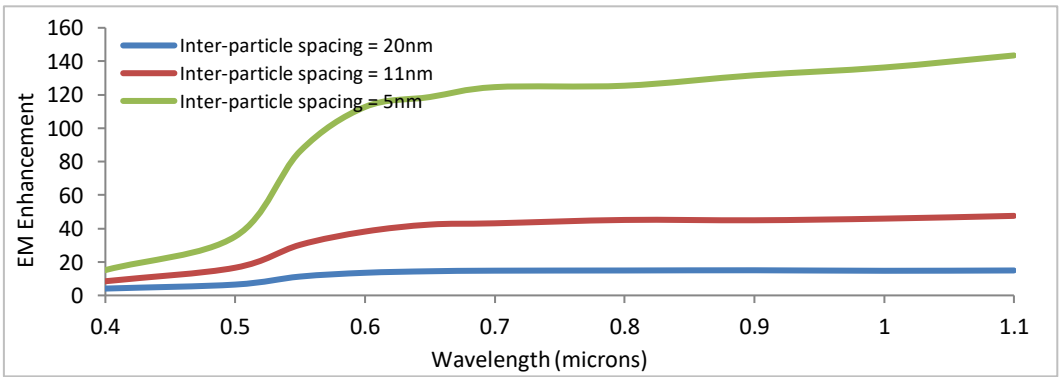

Figure 4.5: EM Enhancement vs. wavelength (periodic boundaries) when the radius of each gold nanospheres is chosen to be 40 nm.

These simulations were repeated by using 'Periodic' boundaries. Periodic boundaries append the unit cell an infinite number of times. Hence, by choosing x

and y boundaries to be periodic, an array containing an infinite number of particles was simulated. The graph illustrating the comparison between the results pertaining to inter-particle spacings of 5nm, 11nm and 20nm is shown in Fig. 4.5

Again, it is observed that as the inter-particle spacing decreases, the field enhancement increases. This observation is consistent with the previous simulations (dimer of gold nanoparticles).

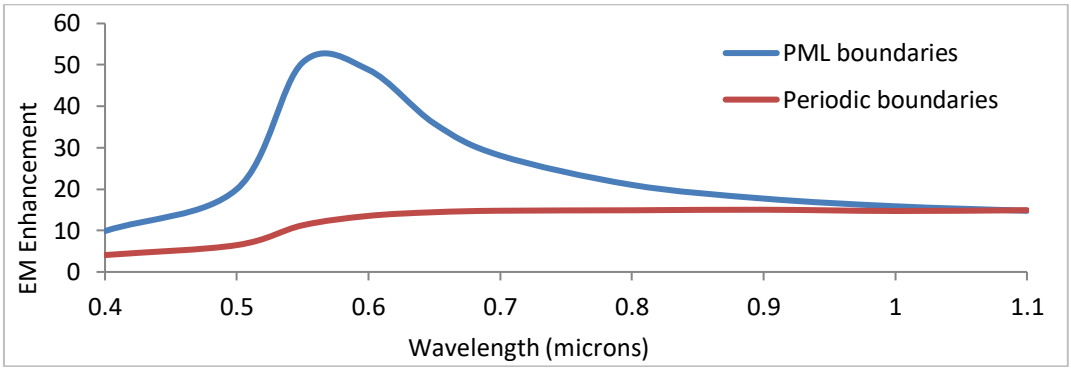

Figure 4.6: Difference in PML boundary simulations and Periodic boundary simulations for inter-particle spacing of 20 nm and radius 40 nm.

Considering the graph illustrating the difference between the results of 'dimer of gold nanoparticle' simulations and 'array of gold nanoparticle' simulations (Fig. 4.6), it can be observed that electric field enhancement in case of an isolated pair of gold nanoparticle is very different from that of an array of gold nanoparticles. This difference can explained as follows: as the number of gold nanoparticles tends to infinity, the electric fields due to oscillating electrons of all the particles interfere. Consequently, a redistribution of electric field takes place and the intensity response changes. This observation is also consistent with the results we obtained for inter-particle spacing of 5 nm and 11 nm as shown in Fig. 4.7.

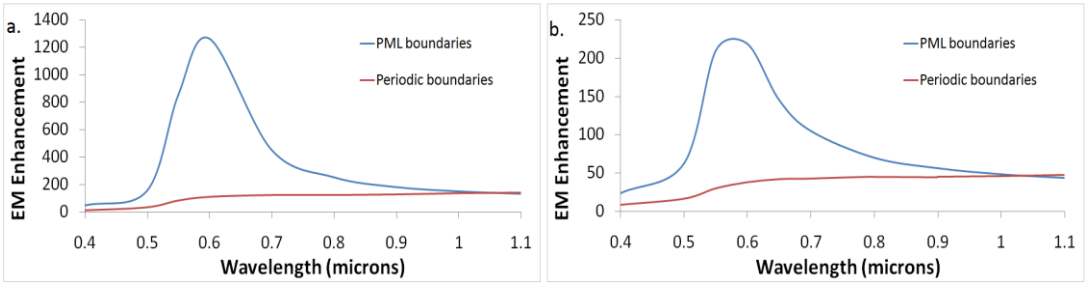

Figure 4.7: Comparison between PML and Periodic boundary simulations for an inter-particle spacing of (a) 5 nm and (b) 11 nm when the radius of each gold nanosphere is 40 nm.

Optical waveguides exploit such coupling effects of a long chain of metal nanoparticles. The study of these coupling effects through simulations might help us develop better optical waveguides.

4.3.4 Bimetallic particles

A nanoparticle composed of two different metals is called a bi-metallic particle. Changing the composition of the nanoparticle changes its dielectric constant and hence its optical properties. This would lead to a change in the resonance spectrum [44]. Consequently, bimetallic particles were simulated during the course of our project in an attempt to observe this change and explore the possibility of passive tunability.

For subsequent simulations, two bi-metallic particles, each consisting of a silver core of radius 20nm, coated with a 20 nm thick gold layer were used. The refractive index profile of the bimetallic particles is shown in Fig. 4.8.

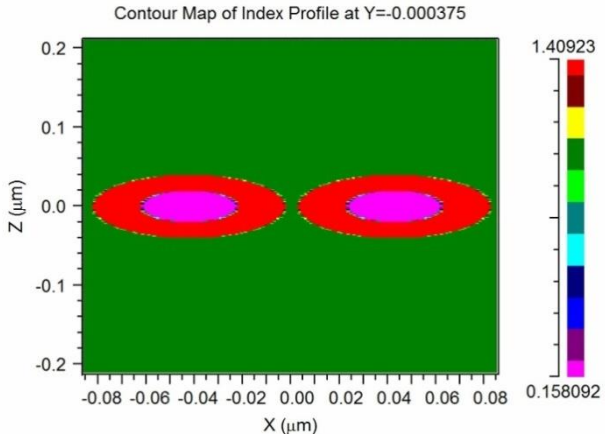

Figure 4.8: Refractive index profile of bimtallic nanospheres at a wavelength of 400 nm. Each particle consists of a silver core of radius 20 nm and a gold coating of thickness 20 nm. The inter-particle distance is 5 nm.

The pink region in the middle is the silver core. The outer red region is the gold coating. Green region is the surrounding vacuum. The EM enhancement vs wavelength for an inter-particle spacing of 5 nm is shown in Fig. 4.9.

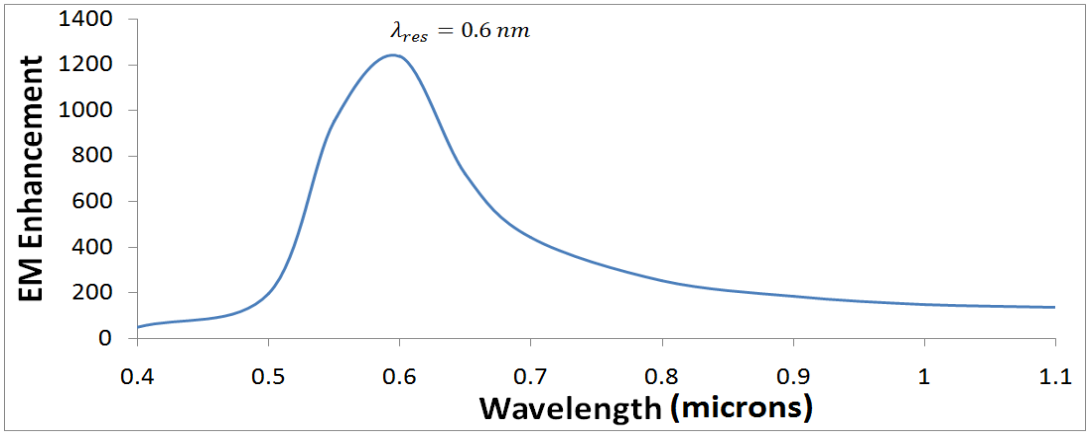

Figure 4.9: EM Enhancement vs wavelength response for a dimer of bi-metallic particles with a silver core of radius 20 nm coated with 20 nm thick gold coating. Inter-particle spacing is chosen to be 5 nm.

The results were compared with those of gold nanoparticles as shown in Fig. 4.10. The wavelength at which resonance occurs seems to have blue-shifted by a small amount in case of bi-metallic particles. In an attempt to observe the blue-shift, these simulations were repeated for the wavelength range 0.55 – 0.6 microns, with a wavelength spacing of 10 nm. The results are shown in Fig. 4.11.

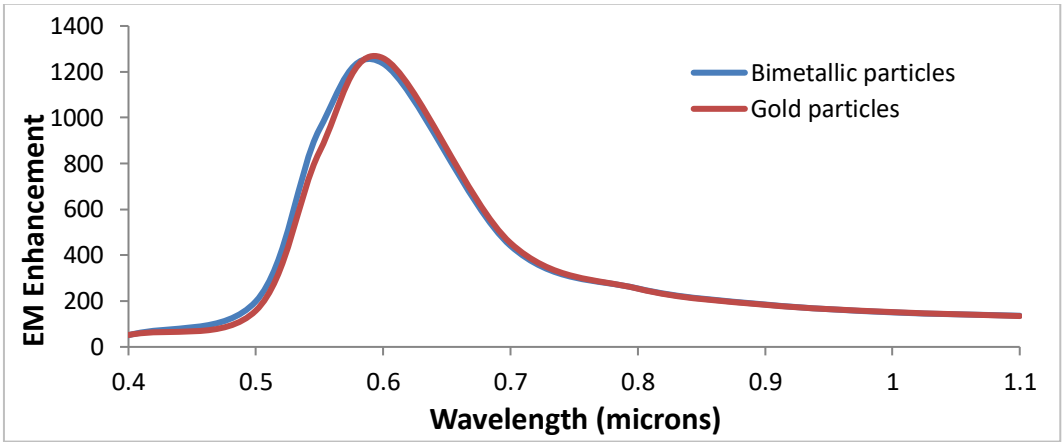

Figure 4.10: Comparison of EM Enhancement of a dimer of bi-metallic nanospheres and gold nanospheres for an inter-particle spacing of 5 nm. The radius of each nanosphere is chosen to be 40 nm.

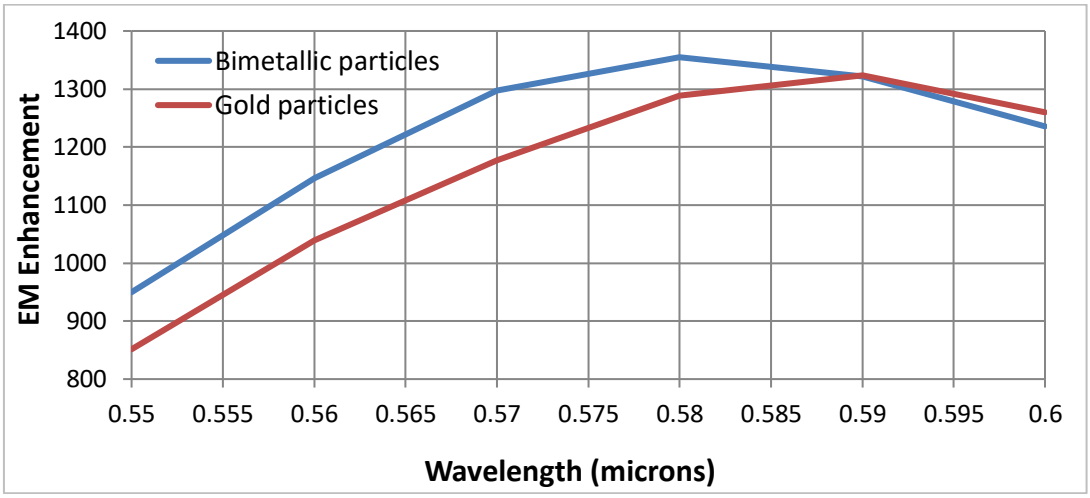

Figure 4.11: Resonance wavelength of bimetallic nanospheres has blue-shifted as compared to the resonance wavelength of gold nanospheres. Gold nanospheres have a radius of 40 nm and an inter-particle distance of 5 nm. Bimetallic nanospheres consist of a silver core of radius 20 nm coated with 20 nm thick gold layer. The inter-particle distance of dimer of bimetallic nanospheres is also 5 nm.

As can be seen, the resonance wavelength has been shifted from 0.59 microns in case of pure gold nanoparticles to 0.58 microns in case of bi-metallic particles. This blue-shift can be explained as follows: as the composition of the metal nanoparticle is changed, the dielectric constant gets altered. Consequently, the wavelength at which the Frohlich condition gets satisfied shifts too. So, a change in dielectric constant would imply a change in polarizability of the dipoles. This would

indicate an altered restoring force on the oscillating electrons. Therefore, the wavelength at which they achieve resonance shifts.

These results are consistent for simulations pertaining to inter-particle spacings of 11 nm and 20 nm as shown in Fig. 4.12.

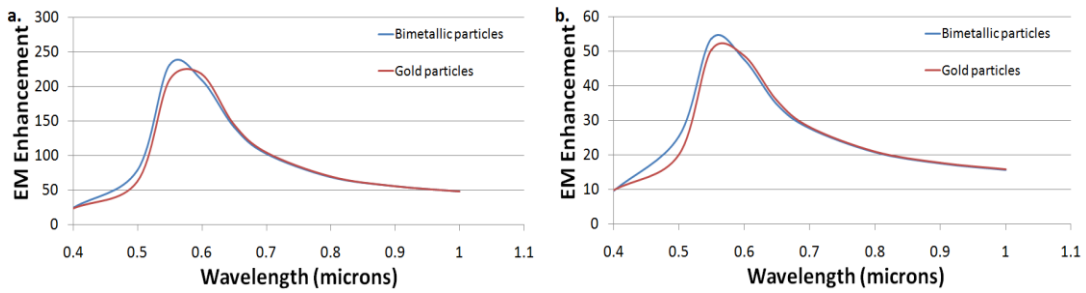

Figure 4.12: Blue-shift in the resonance wavelengths of dimers of gold and bimetallic nanospheres for inter-particle spacing of (a) 11 nm and (b) 20 nm. Gold nanospheres have a radius of 40 nm and an inter-particle distance of 5 nm. Bimetallic nanospheres consist of a silver core of radius 20 nm coated with 20 nm thick gold layer. The inter-particle distance of dimer of bimetallic nanospheres is also 5 nm.

Thus, from the various discussions in this chapter, we can conclude that the resonance wavelength can be passively tuned by changing the composition of metals in these bimetallic nanoparticles, and that this degree of freedom is not available in a pure gold or silver nanoparticle. However, it is advantageous to couple this freedom of passive tenability with high EM enhancements, which can be done by optimizing the shape and size of these bimetallic nanoparticles. In the subsequent chapters, we exploit the lightning rod effect to generate high EM enhancements and discuss novel nanostructures which offer this combined advantage.

CHAPTER 5

PASSIVELY TUNABLE BIMETALLIC NANO-BOWTIES FOR EM ENHANCEMENT

5.1 SUMMARY

It was demonstrated in the previous chapter that bimetallic nanoparticles offer the possibility of passively tuning the resonance wavelength. In this chapter, a detailed study of this tenability has been carried out. Additionally, we propose bimetallic bowtie shaped nanoparticles as it is well known that the triangular shape of these bow-ties generates high EM enhancement. The change in EM enhancement and the resonance wavelength has been studied by varying the various geometrical parameters of these nano-bowties. Moreover, it was found that varying the height of the bowtie structures leads to dual wavelength enhancement, that is, enhancement occurring at two different wavelengths.

5.2 SCHEMATIC OF THE EM ENHANCEMENT STRUCTURE

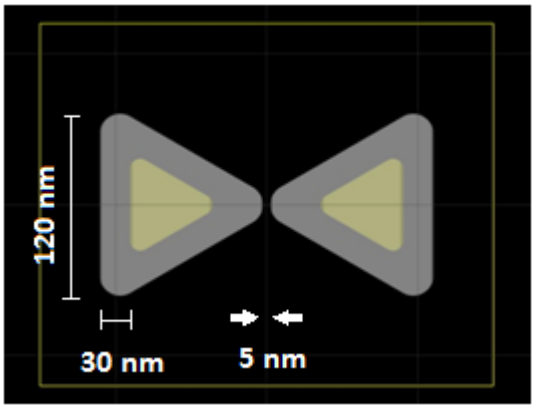

Figure 5.1: Bimetallic bowtie nanoparticles, with a gold core surrounded by silver, separated by a distance of 5 nm, height of 50 nm and surrounded by PML boundaries.

A dimer of bimetallic bowtie nanoparticles (particles consisting of a gold core surrounded by a 30 nm thick layer of silver) separated by a distance of 5nm was simulated. These were illuminated with normally incident light of wavelength

ranging from 0.4 microns to 1 micron. The side length of each particle was taken to be 120 nm and the height was 50 nm. During simulations, the particles were surrounded by 8 layer thick stretched coordinate 'Perfectly Matched Layer' boundaries. The schematic is shown in Fig. 5.1. The yellow boundary represents the monitor that is used to observe the electric field. Light is normally incident on the nanoparticles. Drude-Lorrentz model has been used for gold. Incident light is polarized along the inter-particle axis.

5.3 REULTS AND DICUSSIONS

5.3.1 Dimer of bimetallic nano-bowties with inter-particle distance of 5 nm

For a dimer of bimetallic nano-bowties described in section 5.2, the graph of electric field as a function of wavelength at the exact centre between the two particles, that was obtained is shown in Fig. 5.2.

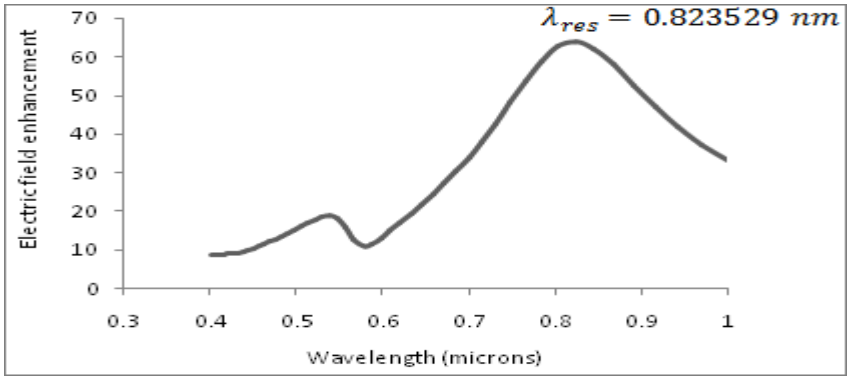

Figure 5.2: Electric field enhancement as a function of wavelength for a dimer of bimetallic bowtie nanoparticles. The side length of the bowtie shaped nanoparticles is 120 nm, height is 50 nm and inter-particle spacing is 5 nm.

It can be seen from the graph, the electric field due to the excitation of Surface Plasmons in bimetallic bowtie nanoparticles is about 63 times more than the incident field (at the resonance wavelength).

5.3.2 Comparison with previous results

In section 4.3.4 the results of bimetallic nano-spheres with diameter of 80 nm and inter-particle distance of 5 nm were described. In this section, bimetallic bowtie nanoparticles, with a side length of 120 nm, height 50 nm and an inter-particle distance of 5 nm are being simulated. Fig. 5.3 contrasts the 2 structures.

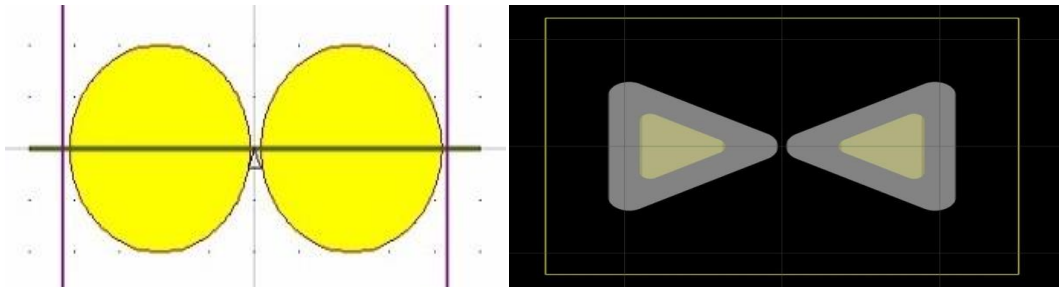

Figure 5.3: Contrast between the two structures.

The electric field observed at the exact centre of these particles is illustrated in Fig. 5.4.

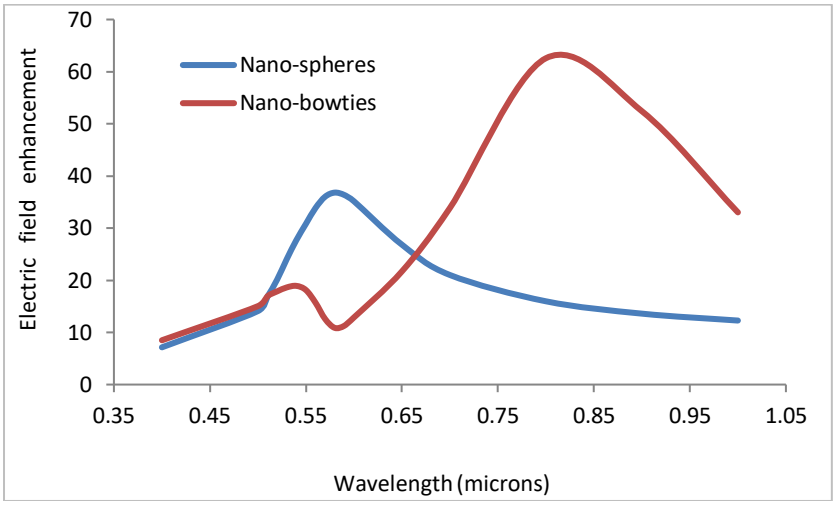

Figure 5.4: Comparison between spectral response of a dimer of nano-spheres and bimetallic bowtie nano-particles. The nanospheres have a diameter of 80 nm and an inter-particle distance of 5 nm. The bowtie shaped nanoparticles have a side length of 120 nm, height 50 nm and inter-particle distance of 5 nm.

It can be seen from the graph, that electric field enhancement in nano-spheres is of the order of 37. On the other hand, the field enhancement in case of bimetallic bowtie structures is of the order of 63. This demonstrates the drastic effect of shape on the spectral response. A small peak in the lower wavelength region for bowtie nano-particle case is also noticed. The nano-spheres had diameter of 80 nm (inter-particle spacing is 5nm). The side length of triangles in bowtie structure is 120 nm. As the particle size increases, the particles start sustaining multipole oscillations, which manifest themselves in the form of small multiple peaks at lower wavelengths.

5.3.3 Varying the thickness of silver coating

The core/shell ratio of our nano-particles was altered by varying the thickness of the silver coating such that the side length of outer triangle remains

constant (with a value of 120 nm). The height was taken to be 50 nm and the inter-particle distance was 5nm. The results are illustrated in Fig. 5.5.

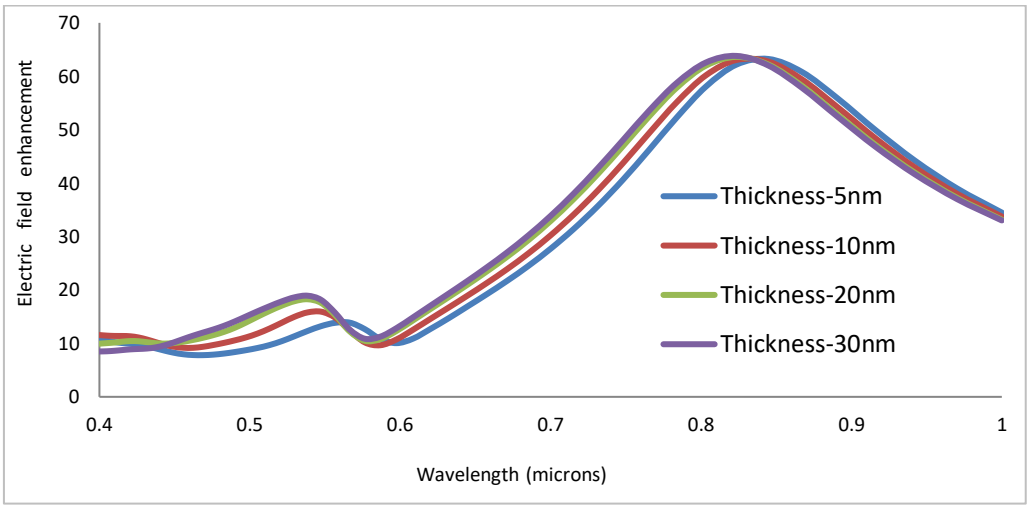

Figure 5.5: Electric field enhancement as a function of wavelength for different core/shell ratios of bimetallic bowtie shaped nanoparticles for a side length of 120 nm, height of 50 nm and inter-particle spacing of 5 nm.

It is observed that as the thickness increases, i.e., as the core/shell ratio decreases, the resonance wavelength blue-shifts.

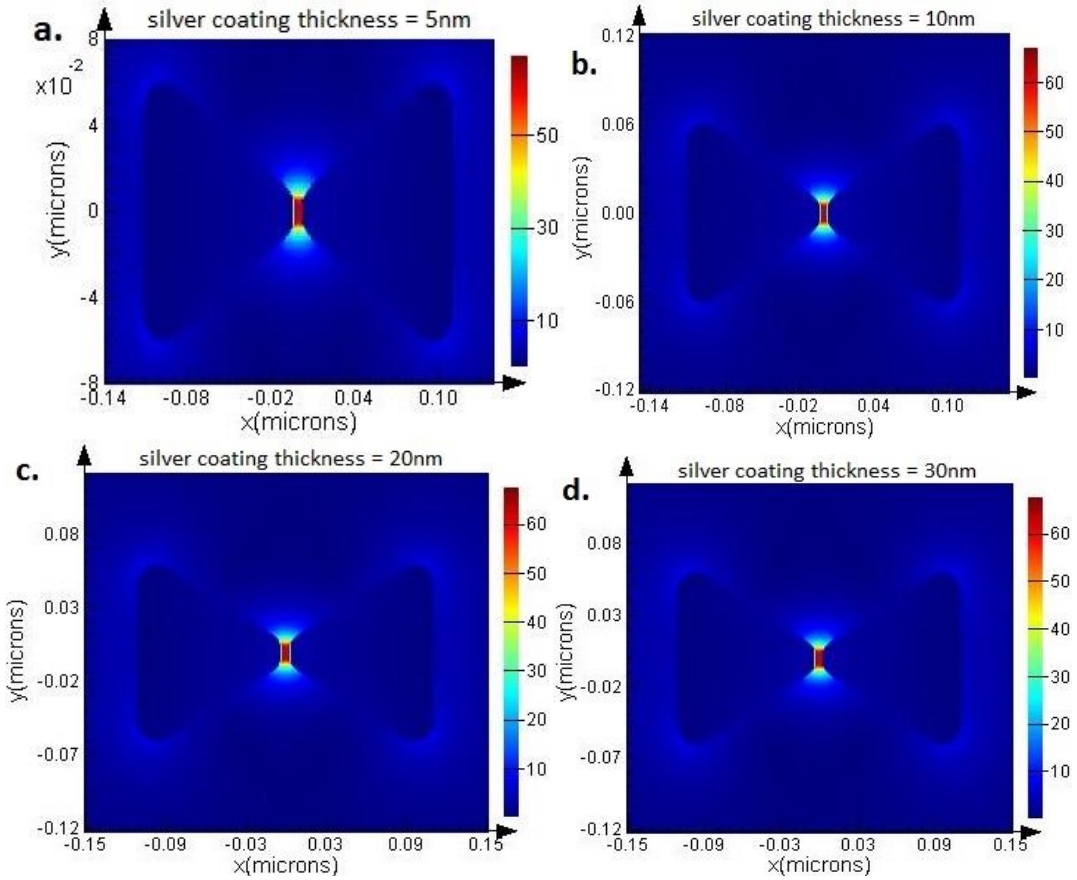

Figure 5.6: Electric field maps of bimetallic bowtie shaped nanoparticles for side length of 120 nm, height of 50 nm, inter-particle distance of 5 nm and silver coating thickness of (a) 5 nm, (b) 10 nm, (c) 20 nm and (d) 30 nm at the resonance wavelength.

A total blue-shift of 21.3 nm as the silver coating is varied from 5 nm to 30 nm is observed. Changing the core/shell ratio alters the optical properties of the nanoparticle due to a change in the effective dielectric constant. Since resonance characteristics depend on the optical response of the nanoparticle, changing the optical properties brings about a change in the resonance characteristics. So, we see that bimetallic particles offer an added advantage of tunability over single metal particles: the resonance curve can be fine tuned by changing the core/shell ratio. The electric field maps are shown in Fig. 5.6.

Hence, passive tunability can be achieved by changing the ratio of the constituent metals in the bimetallic nanoparticle. In chapter 2 of this article, multiple applications have been reviewed where the metal nanoparticles have been used as refractive index sensors. So, by changing the composition of these particles, sensors can be passively tuned to work on different wavelengths.

5.3.4 Varying the side length of the bowties

To explore the possibility of additional tunability, the side length of the bowtie shaped structures was varied. The height of the bowtie shaped pillars was taken to be 50 nm, inter particle spacing was chosen to be 10nm and the silver coating was kept to be 5nm. The results are shown in Fig. 5.7.

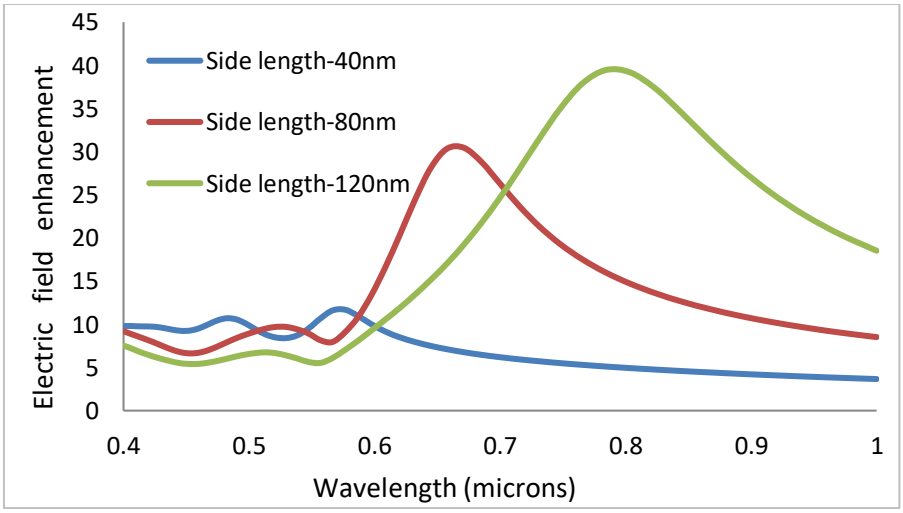

Figure 5.7: Spectral response of bimetallic bowtie shaped nanoparticles for different side lengths with height = 50 nm, inter-particle spacing = 10 nm and silver coating thickness = 5nm.

It can be seen that an increase in side length leads to increase in E field enhancement and a red-shift in resonance wavelength. The expression of polarizability of the dipoles induced is given as [11]:

$$\alpha = 4\pi a^3 \frac{\epsilon - \epsilon_m}{\epsilon + 2\epsilon_m} \tag{5.1}$$

where, a is the radius of the particle, ϵ is the dielectric constant of the nanoparticle and ϵ_m is the dielectric constant of the surrounding dielectric. It can be seen from the above expression that the polarizability is directly proportional to the cube of the radius of the particle. Therefore, larger the particle, the more polarizable are the dipoles and hence the easier it is to polarize them. Consequently, larger the particle, lesser is the energy required to polarize them. That is why, with increasing size, the resonance occurs at lower energy (red-shifts). Additionally, the electric field is directly proportional to the polarizability [11]. Hence, increase in polarizability (due to increase in size) leads to increase in the electric field enhancement. The electric field maps are given in Fig. 5.8.

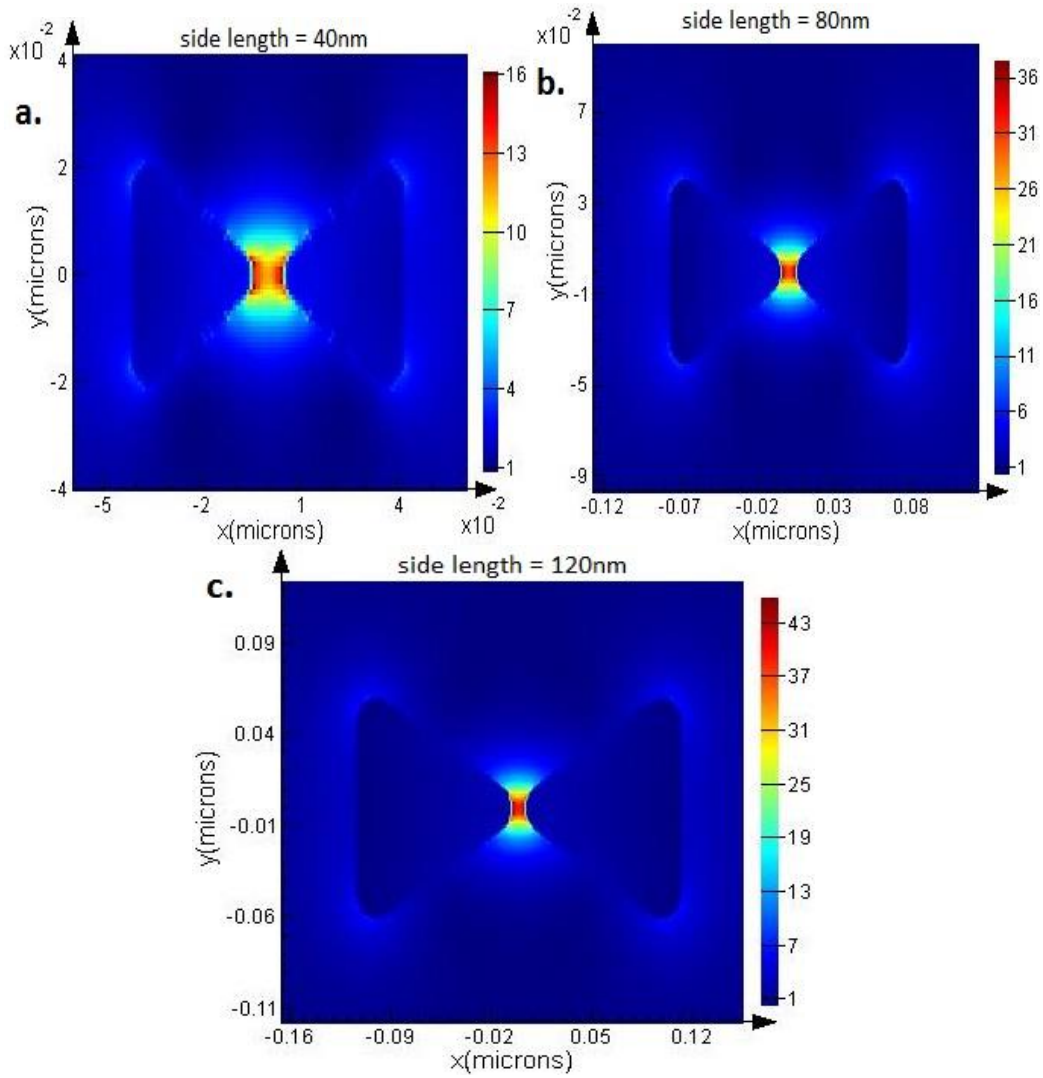

Figure 5.8: Electric field maps of bimetallic bowtie shaped nanoparticles for different side lengths when height = 50 nm, inter-particle spacing = 10 nm and silver coating thickness = 5 nm at the resonance wavelength.

It can be observed that changing the side length of the particle leads to a large shift in the resonance wavelength. Hence, it can be concluded that we can coarse tune the resonance wavelength by changing the size of the particle.

The above conclusions can be applied to achieve refractive index sensing: resonance wavelength can be coarse tuned by varying the side length of the nanoparticles and fine tuned by modifying the core/shell ratio. Consequently, refractive index sensors can be tuned to work at different wavelengths [44].

Additionally, this particular property can be exploited in the field of photovoltaics [14]. As mentioned in section 2.3.1, the efficiency of solar cells can be greatly improved by embedding metal nanoparticles in the depletion region [14]. Solar cells can be configured to absorb different parts of the solar spectra by fine tuning the resonance wavelength of the embedded nanoparticles.

5.3.5 Varying the height of the bowties

The height of the particles was varied keeping the side length to be 120 nm, inter-particle spacing to be 10 nm and silver coating thickness to be 10 nm. The results of the simulations are illustrated in Fig. 5.9.

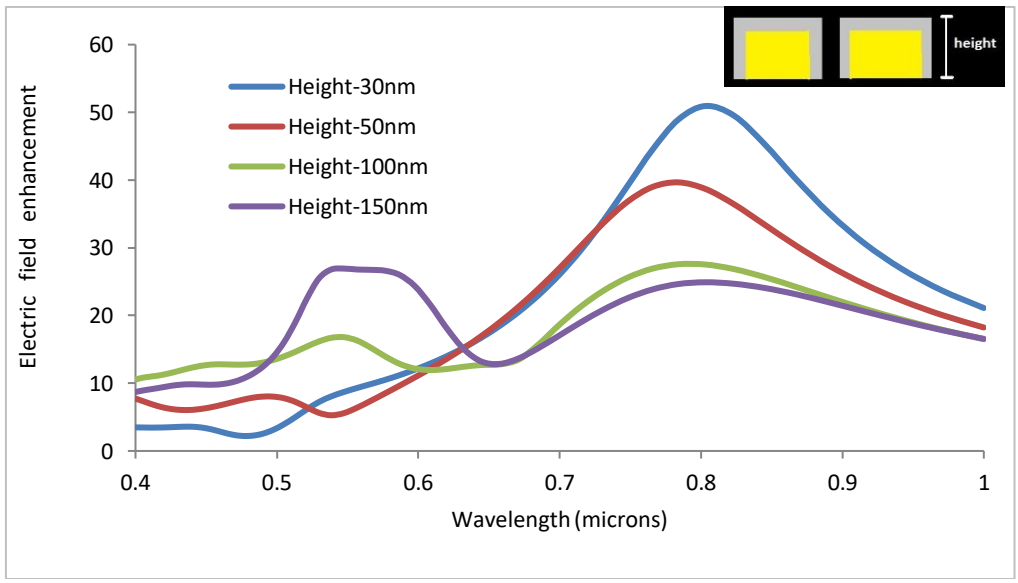

Figure 5.9: Electric field as a function of wavelength of bimetallic bowtie shaped nanoparticles for different heights with side length = 120 nm, inter-particle spacing = 10 nm and silver coating thickness = 10 nm. Inset shows the side view of the nanoparticles.

It can be seen that as the height increases, the electric field enhancement due to dipole resonance decreases and enhancement due to quadrupole resonance increases. This is due to the fact that as the particle height increases, the phase of the

incident wave no longer remains constant over the entire surface of the particle. Consequently, this phase lag between different points on the particle surface leads to multipole oscillations. With increasing height, magnitude of multipole oscillations increases.

It can clearly be seen that there is dual wavelength enhancement: electric field enhancement occurring at two wavelengths. So, we can use the same sensor with two different sources. This, again, gives us flexibility in passively tuning the resonance wavelength. The electric field maps for different heights are shown in Fig. 5.10.

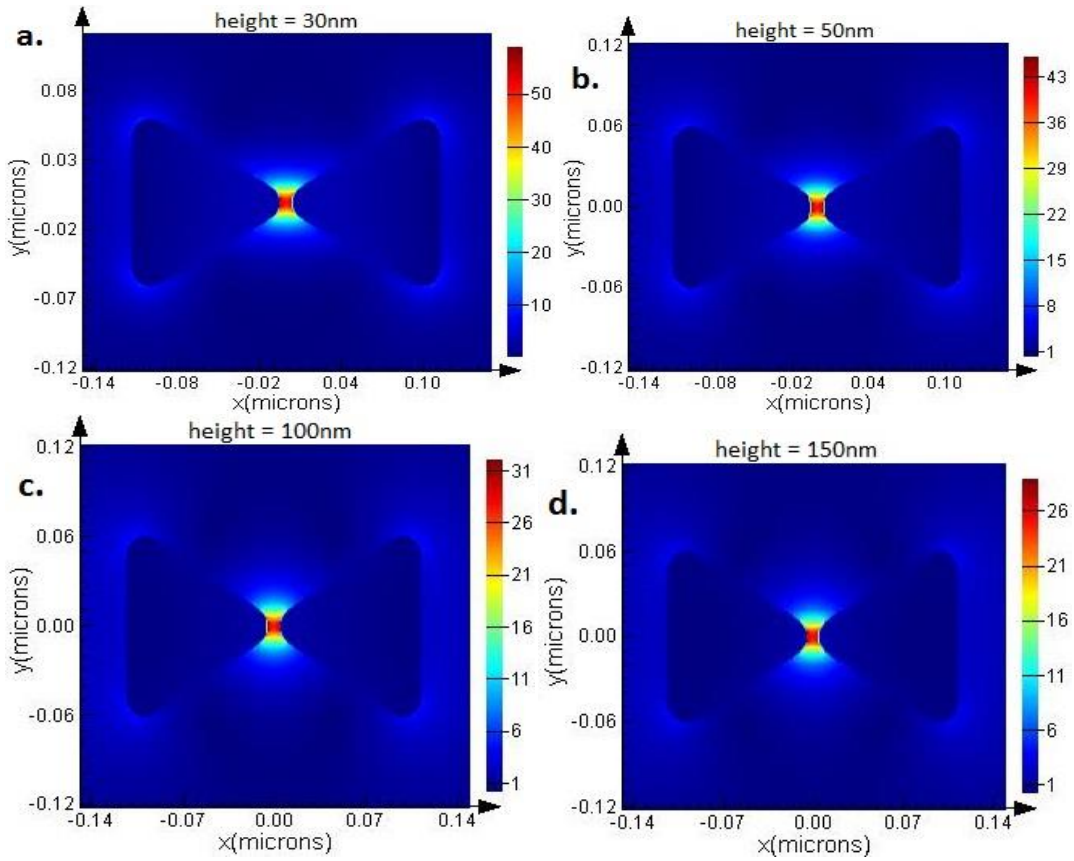

Figure 5.10: Electric field maps of bimetallic bowtie shaped nanoparticles corresponding to different heights at the resonance wavelength.

5.3.6 Varying the inter-particle distance of the bowties

To tune the electric field enhancement, the inter-particle distance between the two nanoparticles was varied. The side length is chosen to be 120 nm. The height is taken to be 50 nm. The thickness of silver coating is kept to be 10 nm. The graph illustrating the results is shown in Fig. 5.11.

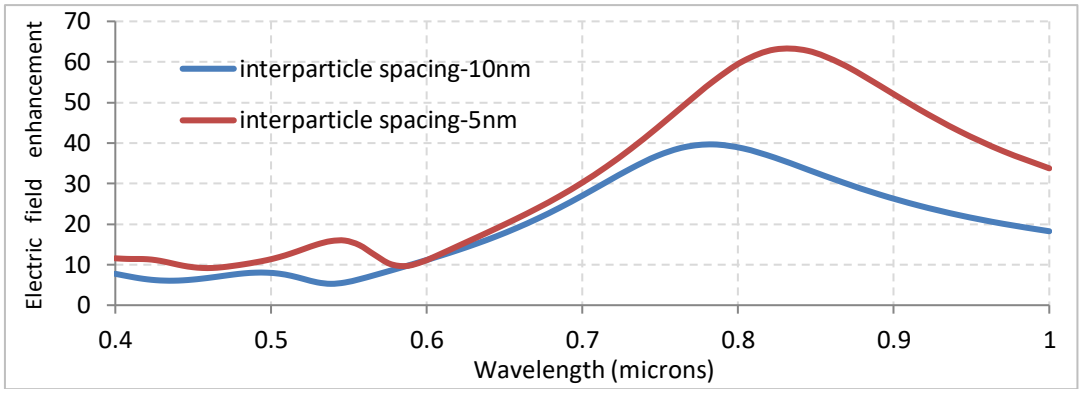

Figure 5.11: Resonance characteristics for different inter-particle spacings of bimetallic bowtie shaped nanoparticles with side length = 120 nm, height = 50 nm and silver coating thickness = 10 nm.

As the particles come closer, the induced dipoles in these nanoparticles interact more strongly producing a high value of electric field enhancement. The electric field maps for different inter-particle spacings are shown in Fig. 5.12.

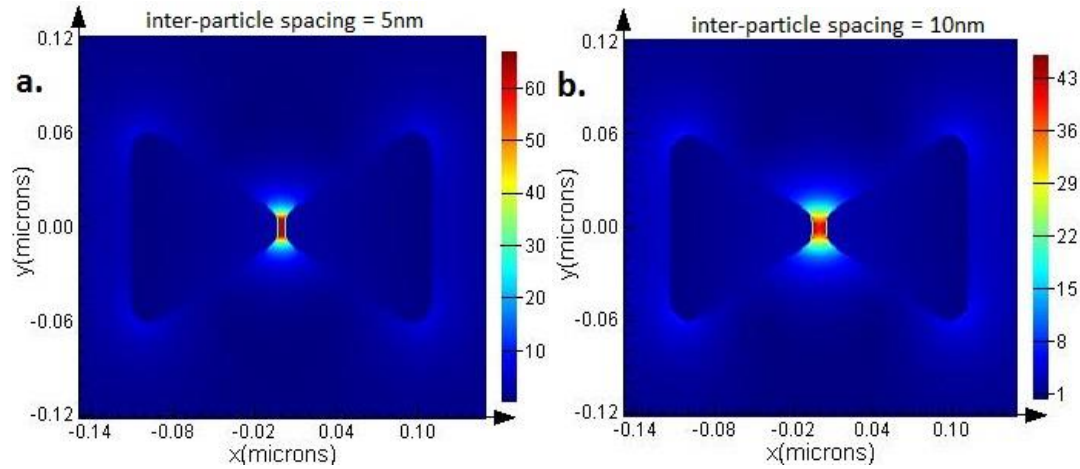

Figure 5.12: Electric field maps of bimetallic bowtie shaped nanoparticles for side length = 120 nm, height = 50 nm, silver coating thickness = 10 nm and inter-particle spacings of (a) 5 nm and (b) 10 nm at the resonance wavelength.

Hence, fine tuning of resonance wavelength has been achieved by varying the core/shell ratio of the bimetallic nanoparticles and coarse tuning has been obtained by varying the side length of the nanoparticle. Additionally, dual wavelength enhancement has also been demonstrated by varying the height of the nanoparticles. In the next chapter we attempt to observe the change in resonance spectrum by breaking the symmetry of dimer of nanoparticles.

CHAPTER 6

HETERO-STRUCTURED BIMETALLIC NANO-BOWTIES

6.1 SUMMARY

In chapter 5, dimers of symmetric bimetallic nano-bowties were simulated. In the simulations discussed in this chapter, we tried to engineer the electric field enhancement by breaking the symmetry of the dimer of bimetallic nano-bowties. These *hetero-structured dimers* consist of asymmetric bimetallic nano bowties as opposed to symmetric bimetallic nano bowties constituting the homo dimers described in the previous chapter. Further, these hetero-structured dimers were simulated for different core/shell ratios and the spectral response was observed.

6.2 SCHEMATIC

The side length of the larger bowtie was kept to be 120 nm and the side length of the smaller bowtie was varied. The height of the bowties is taken to be 50 nm, the inter-particle spacing is chosen to be 5 nm, and the silver coating is 5 nm thick. These hetero-structures are irradiated with electromagnetic radiation of wavelength ranging from 0.4 microns to 1 micron. During simulations, the particles were surrounded by 'Perfectly Matched Layer' boundaries. The schematic is illustrated in Fig. 6.1

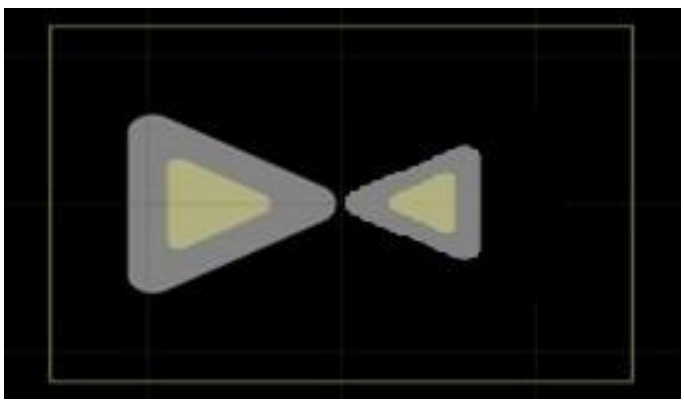

Figure 6.1: Schematic of hetero-structured bimetallic nano-bowties.

6.3 RESULTS AND DISCUSSIONS

Fig. 6.2 illustrates the results. For the ratio of the side length of the smaller triangle and the larger triangle (side length ratio) of 1:1, an electric field enhancement of about 63 is observed. For side length ratio of 1:1.5, it is about 68. The electric field enhancement keeps on decreasing with the further decrease in the side length ratio. Hence, it can be concluded that the side length ratio of 1:1.5 yields the best electric field enhancement for this case. Additionally, it can also be seen that the resonance wavelength keeps on blue-shifting with decreasing side length ratios.

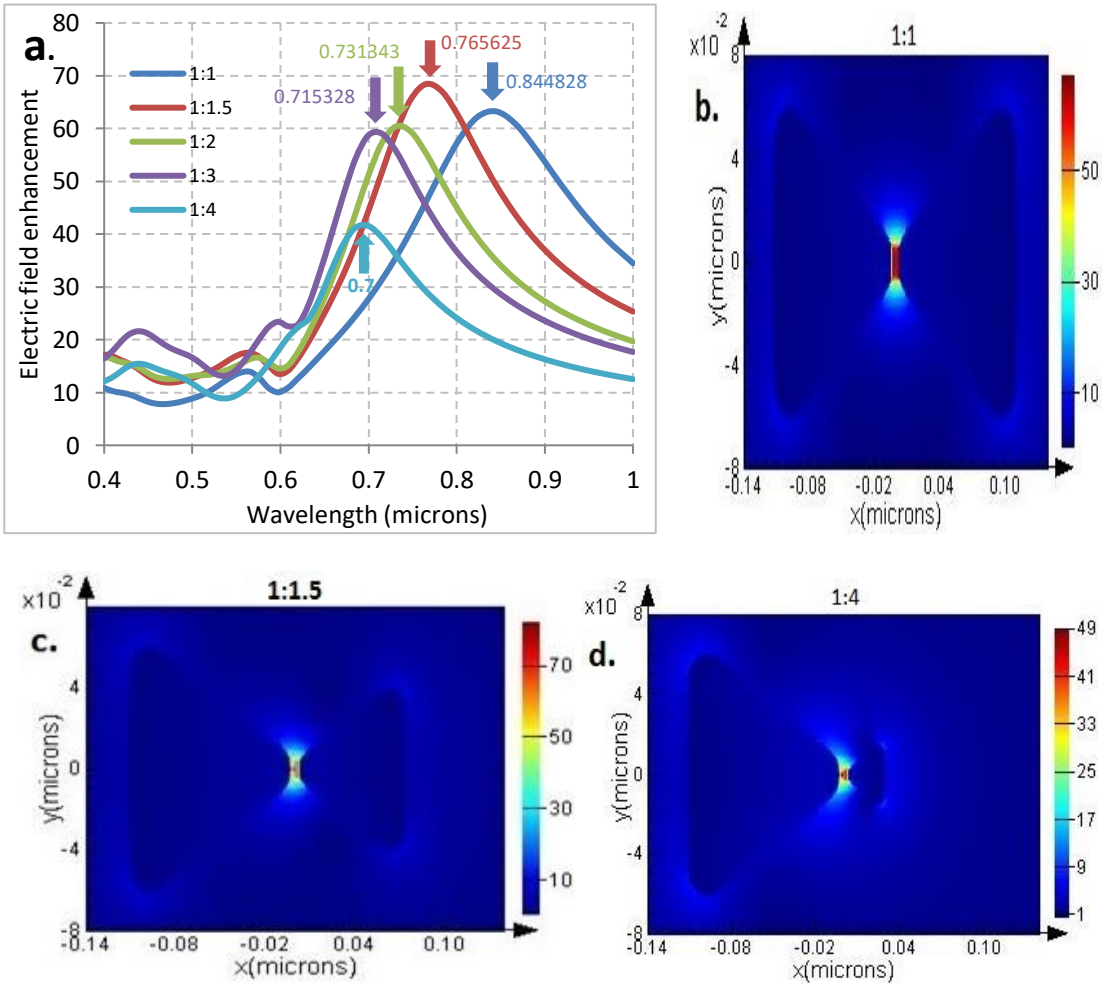

Figure 6.2: (a) Spectral response obtained for hetero-structured bimetallic nano-bowtie when the side length of the larger triangle is kept to be 120 nm and the side length of the smaller triangle is varied. The height of the bowties is taken to be 50 nm, the inter-particle spacing is 5 nm and the silver coating is 5 nm thick. Electric field maps for side length ratios of (b) 1:1, (c) 1:1.5 and (d) 1:4

In Fig. 6.2, for side length ratios of 1:1, 1:1.5 and 1:2, the presence of a second peak around 0.55 microns is observed. This peak is attributed to the bonding mode of quadrupole oscillations. For side length ratios of 1:3 and 1:4, another peak

around 0.45 microns is observed. It is known that [45], the antibonding mode of dipole oscillations occurs at lower energy (higher wavelength) than the antibonding mode of quadrupole oscillations. Hence, this could be attributed to the antibonding mode of dipole oscillations.

Fig. 6.3 illustrates the results for decreasing side length ratios when silver coating thickness is chosen to be 10 nm, 20 nm and 30 nm. The other parameters remain unchanged. It can be noticed that the electric field enhancement is about 63 for the side length ratio of 1:1. It keeps on decreasing with decreasing side length ratios. Hence, for silver coating thickness 10 nm and above, a side length ratio of 1:1 yields the best field enhancement. This is in contrast with the results obtained for a silver coating thickness of 5 nm (Fig. 6.2).

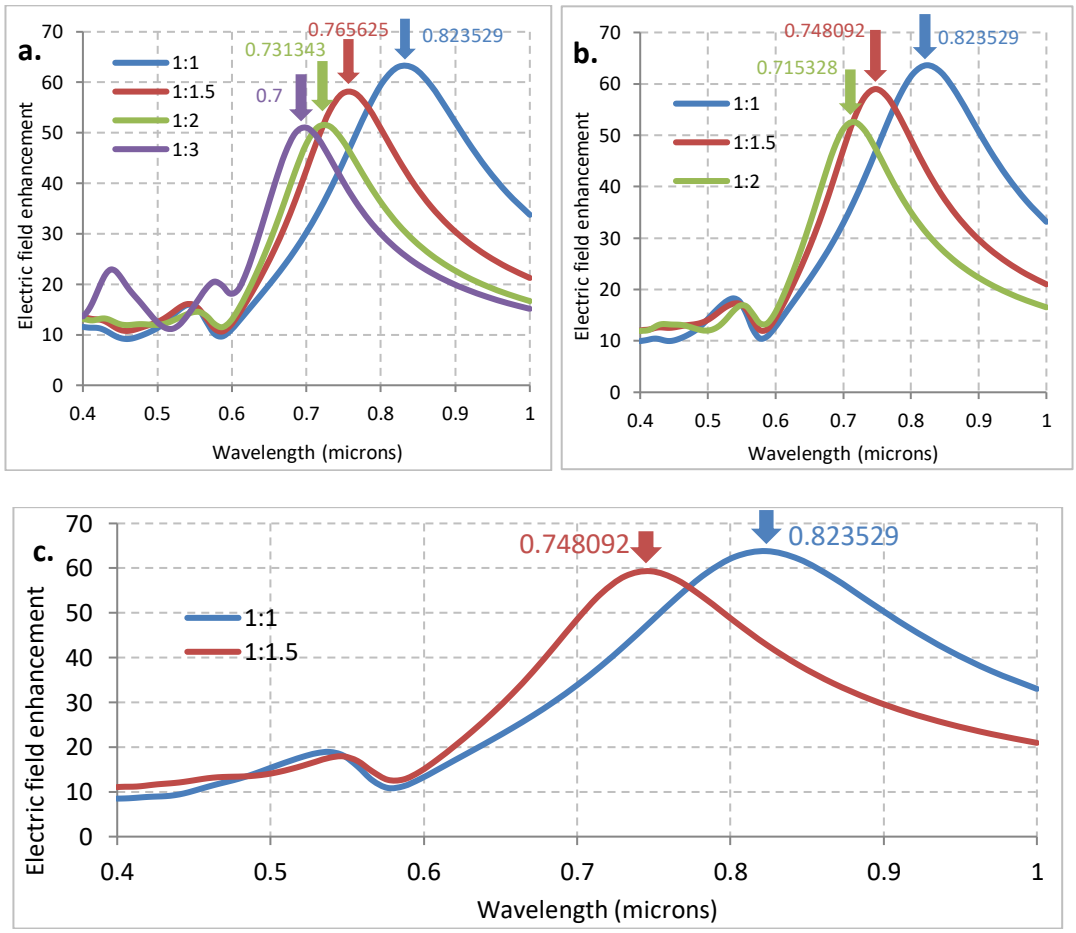

Figure 6.3: Spectral response of hetero-structured bimetallic nano-bowtie for variable side length ratios when side length of the larger triangle is 120 nm, height is 50 nm, inter-particle spacing is 5 nm and silver coating thickness is (a) 10 nm, (b) 20 nm and (c) 30 nm.

Additionally, a blue-shift in the resonance wavelength with decreasing side length ratios can be observed which is in agreement with the results of Fig. 6.2. Also, the presence of bonding hybridized mode of quadrupole oscillations can be

seen for side length ratios of 1:1, 1:1.5 and 1:2 and antibonding mode of dipole oscillations for side length ratio of 1:3, along with the bonding mode of dipole oscillations. Again, this agrees with the results of Fig. 6.2.

CHAPTER 7

CONCLUSIONS AND FUTURE WORK

In the first two chapters of the thesis, the phenomenon of Localized Surface Plasmon Resonance has been reviewed from a physical and mathematical perspective. Multiple applications of Localized Surface Plasmon Resonance in metal nanoparticles have been reviewed in the third chapter. The Finite Difference Time Domain method has been discussed in the fourth chapter. Through the course of this project, multiple FDTD simulations have been done in an attempt to study the plasmonic properties of metal nanoparticles and explore the prospect of passive tunability. The results have been analyzed in subsequent chapters. The drastic effect of shape and size of the nanoparticles on the resonance spectrum has been demonstrated. The difference in the resonance spectrum of an isolated pair of nanoparticles and an array of nanoparticles has also been illustrated. It has been shown that varying the side length of the nanoparticles helps in coarse tuning the resonance wavelength and changing the core/shell ratio of the bimetallic nanoparticles helps in fine tuning the resonance wavelength. A total fine tuning of 21.3 nm has been achieved by varying the core/shell ratio. It is advantageous to couple this degree of freedom (of passive tunability) with high EM enhancements. Consequently, homo-structured and hetero-structured bowtie shaped nanoparticles have been simulated in attempt to achieve high EM enhancement. Maximum EM enhancement (of about 68) has been observed for side length ratio of 1:1.5, where the side length of the nanoparticle is chosen to be 120 nm, height is taken to be 50 nm, inter-particle distance to be 5 nm and silver coating thickness is kept as 5 nm.

As the next step, fabrication of these nanostructures can be attempted. Other nanostructures that offer higher EM enhancement can be simulated. Additional structures with asymmetric features can be explored. Publication of the work presented in this thesis can also be done. Nanoshells or tri-metallic nanoparticles can also be simulated in order to study their plasmonic properties.

REFERENCES

[1] Prasad, P. N. (2004). *Nanophotonics*. John Wiley & Sons.

[2] Kiefer, W. (2011). *Surface enhanced Raman spectroscopy: analytical, biophysical and life science applications*. John Wiley & Sons.

[3] Evanoff, D. D., & Chumanov, G. (2005). Synthesis and optical properties of silver nanoparticles and arrays. *ChemPhysChem*, *6*(7), 1221-1231.

[4] Hu, M., Chen, J., Li, Z. Y., Au, L., Hartland, G. V., Li, X., ... & Xia, Y. (2006). Gold nanostructures: engineering their plasmonic properties for biomedical applications. *Chemical Society Reviews*, *35*(11), 1084-1094.

[5] Maier, S. A., & Atwater, H. A. (2005). Plasmonics: Localization and guiding of electromagnetic energy in metal/dielectric structures. *Journal of applied physics*, *98*(1), 10.

[6] Srivastava, A. K., Yadev, R., Rai, V. N., Ganguly, T., & Deb, S. K. (2012, June). Surface plasmon resonance in gold nanoparticles. In *AIP Conference Proceedings* (Vol. 1447, No. 1, pp. 305-306). AIP.

[7] Tseng, A. A., Chen, K., Chen, C. D., & Ma, K. J. (2003). Electron beam lithography in nanoscale fabrication: recent development. *IEEE Transactions on electronics packaging manufacturing*, *26*(2), 141-149.

[8] Tseng, A. A. (2005). Recent developments in nanofabrication using focused ion beams. *Small*, *1*(10), 924-939.

[9] Hulteen, J. C., & Van Duyne, R. P. (1995). Nanosphere lithography: A materials general fabrication process for periodic particle array surfaces. *Journal of Vacuum Science & Technology A: Vacuum, Surfaces, and Films*, *13*(3), 1553-1558.

[10] Wagner, C., & Harned, N. (2010). EUV lithography: Lithography gets extreme. *Nature Photonics*, *4*(1), 24.

[11] Maier, S. A. (2007). *Plasmonics: fundamentals and applications*. Springer Science & Business Media.

[12] Mock, J. J., Barbic, M., Smith, D. R., Schultz, D. A., & Schultz, S. (2002). Shape effects in plasmon resonance of individual colloidal silver nanoparticles. *The Journal of Chemical Physics*, *116*(15), 6755-6759.

[13] Zielińska-Jurek, A. (2014). Progress, challenge, and perspective of bimetallic TiO 2-based photocatalysts. *Journal of Nanomaterials*, *2014*, 3.

[14] Atwater, H. A., & Polman, A. (2010). Plasmonics for improved photovoltaic devices. *Nature materials*, *9*(3), 205.

[15] Yablonovitch, E., & Cody, G. D. (1982). Intensity enhancement in textured optical sheets for solar cells. *IEEE Transactions on Electron Devices*, *29*(2), 300-305.

[16] Deckman, H. W., Roxlo, C. B., & Yablonovitch, E. (1983). Maximum statistical increase of optical absorption in textured semiconductor films. *Optics letters*, *8*(9), 491-493.

[17] Haes, A. J., Hall, W. P., Chang, L., Klein, W. L., & Van Duyne, R. P. (2004). A localized surface plasmon resonance biosensor: First steps toward an assay for Alzheimer's disease. *Nano letters*, *4*(6), 1029-1034.

[18] Vasileva, P., Donkova, B., Karadjova, I., & Dushkin, C. (2011). Synthesis of starch-stabilized silver nanoparticles and their application as a surface plasmon resonance-based sensor of hydrogen peroxide. *Colloids and Surfaces A: Physicochemical and Engineering Aspects*, *382*(1-3), 203-210.

[19] Verma, R., & Gupta, B. D. (2015). Detection of heavy metal ions in contaminated water by surface plasmon resonance based optical fibre sensor using conducting polymer and chitosan. *Food chemistry*, *166*, 568-575.

[20] Quinten, M., Leitner, A., Krenn, J. R., & Aussenegg, F. R. (1998). Electromagnetic energy transport via linear chains of silver nanoparticles. *Optics letters*, *23*(17), 1331-1333.

[21] Maier, S. A., Kik, P. G., Atwater, H. A., Meltzer, S., Harel, E., Koel, B. E., & Requicha, A. A. (2003). Local detection of electromagnetic energy transport below the diffraction limit in metal nanoparticle plasmon waveguides. *Nature materials*, *2*(4), 229.

[22] Zia, R., Selker, M. D., Catrysse, P. B., & Brongersma, M. L. (2004). Geometries and materials for subwavelength surface plasmon modes. *JOSA A*, *21*(12), 2442-2446.

[23] Krasavin, A. V., & Zheludev, N. I. (2004). Active plasmonics: Controlling signals in Au/Ga waveguide using nanoscale structural transformations. *Applied Physics Letters*, *84*(8), 1416-1418.

[24] Zhu, Z., Feng, M., Zuo, L., Zhu, Z., Wang, F., Chen, L., ... & Luo, S. Z. (2015). An aptamer based surface plasmon resonance biosensor for the detection of ochratoxin A in wine and peanut oil. *Biosensors and Bioelectronics*, *65*, 320-326.

[25] Okamoto, K., Niki, I., Shvartser, A., Narukawa, Y., Mukai, T., & Scherer, A. (2004). Surface-plasmon-enhanced light emitters based on InGaN quantum wells. *Nature materials*, *3*(9), 601.

[26] Hill, M. T., Oei, Y. S., Smalbrugge, B., Zhu, Y., De Vries, T., Van Veldhoven, P. J., ... & Geluk, E. J. (2007). Lasing in metallic-coated nanocavities. *Nature Photonics*, *1*(10), 589.

[27] Oulton, R. F., Sorger, V. J., Zentgraf, T., Ma, R. M., Gladden, C., Dai, L., ... & Zhang, X. (2009). Plasmon lasers at deep subwavelength scale. *Nature*, *461*(7264), 629.

[28] Boyd, G. T., Yu, Z. H., & Shen, Y. R. (1986). Photoinduced luminescence from the noble metals and its enhancement on roughened surfaces. Physical Review B, 33(12), 7923.

[29] Beversluis, M. R., Bouhelier, A., & Novotny, L. (2003). Continuum generation from single gold nanostructures through near-field mediated intraband transitions. Physical Review B, 68(11), 115433.

[30] Schuck, P. J., Fromm, D. P., Sundaramurthy, A., Kino, G. S., & Moerner, W. E. (2005). Improving the mismatch between light and nanoscale objects with gold bowtie nanoantennas. Physical review letters, 94(1), 017402.

[31] Fromm, D. P., Sundaramurthy, A., Schuck, P. J., Kino, G., & Moerner, W. E. (2004). Gap-dependent optical coupling of single “bowtie” nanoantennas resonant in the visible. Nano letters, 4(5), 957-961.

[32] Crozier, K. B., Sundaramurthy, A., Kino, G. S., & Quate, C. F. (2003). Optical antennas: Resonators for local field enhancement. Journal of Applied Physics, 94(7), 4632-4642.

[33] Muehlschlegel, P., Eisler, H. J., Martin, O. J., Hecht, B., & Pohl, D. W. (2005). Resonant optical antennas. science, 308(5728), 1607-1609.

[34] Prangsma, J. C., Kern, J., Knapp, A. G., Grossmann, S., Emmerling, M., Kamp, M., & Hecht, B. (2012). Electrically connected resonant optical antennas. Nano letters, 12(8), 3915-3919.

[35] Kern, J., Kullock, R., Prangsma, J., Emmerling, M., Kamp, M., & Hecht, B. (2015). Electrically driven optical antennas. Nature Photonics, 9(9), 582.

[36] Cubukcu, E., Kort, E. A., Crozier, K. B., & Capasso, F. (2006). Plasmonic laser antenna. Applied Physics Letters, 89(9), 093120.

[37] Hecht, B., Muehlschlegel, P., Farahani, J. N., Eisler, H. J., Pohl, D. W., Martin, O. J., & Biagioni, P. (2006). Prospects of resonant optical antennas for nano-analysis. CHIMIA International Journal for Chemistry, 60(11), 765-769.

[38] Novotny, L. (2007). Effective wavelength scaling for optical antennas. Physical Review Letters, 98(26), 266802.

[39] Alaverdyan, Y., Sepúlveda, B., Eurenius, L., Olsson, E., & Käll, M. (2007). Optical antennas based on coupled nanoholes in thin metal films. Nature Physics, 3(12), 884.

[40] Li, J., & Engheta, N. (2007). Core-shell nanowire optical antennas fed by slab waveguides. IEEE Transactions on Antennas and Propagation, 55(11), 3018-3026.

[41] Prodan, E., Radloff, C., Halas, N. J., & Nordlander, P. (2003). A hybridization model for the plasmon response of complex nanostructures. *science*, *302*(5644), 419-422.

[42] Taflove, A., & Hagness, S. C. (2005). *Computational electrodynamics: the finite-difference time-domain method*. Artech house.

[43] Sadiku, M. N. (2000). *Numerical techniques in electromagnetics*. CRC press.

[44] Gong, C., & Leite, M. S. (2016). Noble metal alloys for plasmonics. *ACS Photonics*, *3*(4), 507-513.

[45] Lassiter, J. B., Aizpurua, J., Hernandez, L. I., Brandl, D. W., Romero, I., Lal, S., ... & Halas, N. J. (2008). Close encounters between two nanoshells. *Nano letters*, *8*(4), 1212-1218.

[46] Lamprecht, B., Schider, G., Lechner, R. T., Ditlbacher, H., Krenn, J. R., Leitner, A., & Aussenegg, F. R. (2000). Metal nanoparticle gratings: influence of dipolar particle interaction on the plasmon resonance. *Physical review letters*, *84*(20), 4721.

[47] Pelton, M., Aizpurua, J., & Bryant, G. (2008). Metal-nanoparticle plasmonics. *Laser & Photonics Reviews*, *2*(3), 136-159.

[48] Félidj, N., Aubard, J., Lévi, G., Krenn, J. R., Hohenau, A., Schider, G., ... & Aussenegg, F. R. (2003). Optimized surface-enhanced Raman scattering on gold nanoparticle arrays. *Applied Physics Letters*, *82*(18), 3095-3097.

[49] Cacciola, A., Iatì, M. A., Saija, R., Borghese, F., Denti, P., Maragò, O. M., & Gucciardi, P. G. (2017). Spectral shift between the near-field and far-field optoplasmonic response in gold nanospheres, nanoshells, homo- and hetero-dimers. *Journal of Quantitative Spectroscopy and Radiative Transfer*, *195*, 97-106.

[50] Ritchie, R. H. (1957). Plasma losses by fast electrons in thin films. *Physical Review*, *106*(5), 874.

[51] Raether, H. (2013). *Surface plasmons on smooth and rough surfaces and on gratings*. Springer-Verlag Berlin An.

[52] Lakowicz, J. R. (2006). Plasmonics in biology and plasmon-controlled fluorescence. *Plasmonics*, *1*(1), 5-33.

[53] Koenderink, A. F., & Polman, A. (2006). Complex response and polariton-like dispersion splitting in periodic metal nanoparticle chains. *Physical Review B*, *74*(3), 033402.

[54] Brongersma, M. L., Hartman, J. W., & Atwater, H. A. (2000). Electromagnetic energy transfer and switching in nanoparticle chain arrays below the diffraction limit. *Physical Review B*, *62*(24), R16356.

[55] Fang, Y., & Sun, M. (2015). Nanoplasmonic waveguides: towards applications in integrated nanophotonic circuits. *Light: Science & Applications*, *4*(6), e294.

[56] Li, K., Stockman, M. I., & Bergman, D. J. (2003). Self-similar chain of metal nanospheres as an efficient nanolens. *Physical review letters*, *91*(22), 227402.

[57] Challener, W. A., Gage, E., Itagi, A., & Peng, C. (2006). Optical transducers for near field recording. *Japanese journal of applied physics*, *45*(8S), 6632.

[58] Kats, M. A., Blanchard, R., Genevet, P., Yang, Z., Qazilbash, M. M., Basov, D. N., ... & Capasso, F. (2013). Thermal tuning of mid-infrared plasmonic antenna arrays using a phase change material. *Optics letters*, *38*(3), 368-370.

[59] Stipe, B. C., Strand, T. C., Poon, C. C., Balamane, H., Boone, T. D., Katine, J. A., ... & Hellwig, O. (2010). Magnetic recording at 1.5 Pb m− 2 using an integrated plasmonic antenna. *Nature photonics*, *4*(7), 484.

[60] Matsumoto, T., Shimano, T., Saga, H., Sukeda, H., & Kiguchi, M. (2004). Highly efficient probe with a wedge-shaped metallic plate for high density near-field optical recording. *Journal of applied physics*, *95*(8), 3901-3906.

[61] Earl, S. K., James, T. D., Davis, T. J., McCallum, J. C., Marvel, R. E., Haglund, R. F., & Roberts, A. (2013). Tunable optical antennas enabled by the phase transition in vanadium dioxide. *Optics express*, *21*(22), 27503-27508.

[62] Beenakker, C. W. J., & Schönenberger, C. (2003). Quantum shot noise. *Physics Today*, *56*(5), 37-42.

[63] Şendur, K., & Challener, W. (2003). Near-field radiation of bow-tie antennas and apertures at optical frequencies. *Journal of microscopy*, *210*(3), 279-283.

[64] Kappeler, R., Erni, D., Xudong, C., & Novotny, L. (2007). Field computations of optical antennas. *Journal of Computational and Theoretical Nanoscience*, *4*(3), 686-691.

[65] Sharma, Y., & Dhawan, A. (2016). Plasmonic “nano-fingers on nanowires” as sers substrates. *Optics letters*, *41*(9), 2085-2088.

[66] Lesuffleur, A., Kumar, L. K. S., Brolo, A. G., Kavanagh, K. L., & Gordon, R. (2007). Apex-enhanced Raman spectroscopy using double-hole arrays in a gold film. *The Journal of Physical Chemistry C*, *111*(6), 2347-2350.

[67] Min, Q., Santos, M. J. L., Girotto, E. M., Brolo, A. G., & Gordon, R. (2008). Localized Raman enhancement from a double-hole nanostructure in a metal film. *The Journal of Physical Chemistry C*, *112*(39), 15098-15101.

[68] Mutlu, M., Kang, J. H., Raza, S., Schoen, D., Zheng, X., Kik, P. G., & Brongersma, M. L. (2018). Thermoplasmonic ignition of metal nanoparticles. *Nano letters*, *18*(3), 1699-1706.

[69] Goswami, A., Aravindan, S., & Rao, P. V. (2016). Fabrication of substrate supported bimetallic nanoparticles and their optical characterization through reflection spectra. *Superlattices and Microstructures*, *91*, 252-258.

[70] Olmon, R. L., Slovick, B., Johnson, T. W., Shelton, D., Oh, S. H., Boreman, G. D., & Raschke, M. B. (2012). Optical dielectric function of gold. *Physical Review B*, *86*(23), 235147.

[71] Boreman, G. D., Johnson, T., Jones, A. C., Oh, S. H., Olmon, R. L., Raschke, M. B., ... & Slovick, B. (2011, May). Broadband electrical permittivity of gold for plasmonics and nano-optics applications. In *Quantum Electronics and Laser Science Conference* (p. QTuL3). Optical Society of America.

[72] Kiefer, W. (2011). *Surface enhanced Raman spectroscopy: analytical, biophysical and life science applications*. John Wiley & Sons.

[73] Oubre, C., & Nordlander, P. (2005). Finite-difference time-domain studies of the optical properties of nanoshell dimers. *The Journal of Physical Chemistry B*, *109*(20), 10042-10051.

[74] Meier, M., Wokaun, A., & Liao, P. F. (1985). Enhanced fields on rough surfaces: dipolar interactions among particles of sizes exceeding the Rayleigh limit. *JOSA B*, *2*(6), 931-949.

[75] Talley, C. E., Jackson, J. B., Oubre, C., Grady, N. K., Hollars, C. W., Lane, S. M., ... & Halas, N. J. (2005). Surface-enhanced Raman scattering from individual Au nanoparticles and nanoparticle dimer substrates. *Nano letters*, *5*(8), 1569-1574.

[76] Sheikholeslami, S., Jun, Y. W., Jain, P. K., & Alivisatos, A. P. (2010). Coupling of optical resonances in a compositionally asymmetric plasmonic nanoparticle dimer. *Nano letters*, *10*(7), 2655-2660.

[77] Li, Z. Y., Wilcoxon, J. P., Yin, F., Chen, Y., Palmer, R. E., & Johnston, R. L. (2008). Structures and optical properties of 4–5 nm bimetallic AgAu nanoparticles. *Faraday discussions*, *138*, 363-373.